Escuela Politécnica Superior de Jaén

Grado en Ingeniería Mecánica

UNIVERSIDAD DE JAÉN

Escuela Politécnica Superior de Jaén

Trabajo Fin de Grado

EXPERIMENTAL STUDY OF THE INFLUENCE OF A VERTICAL WALL ON A RISING BUBBLE

Alumno: Cecilia Estepa Cantero

Tutor: Mª Rocío Bolaños Jiménez
Jesús Carlos Martínez Bazán

Dpto: Ingeniería mecánica y minera

Junio, 2019

Universidad de Jaén
Escuela Politécnica Superior de Jaén
Departamento de Ingeniería Mecánica y Minera

Doña Mª Rocío Bolaños Jiménez y Don Jesús Carlos Martínez Bazán , tutores del Proyecto Fin de Carrera titulado: Experimental study of the influence of a vertical wall on a rising bubble, que presenta Cecilia Estepa Cantero, autorizan su presentación para defensa y evaluación en la Escuela Politécnica Superior de Jaén.

Jaén, junio de 2019

La alumna: Los tutores:

Cecilia Estepa Cantero

Mª Rocío Bolaños Jiménez

Jesús Carlos Martínez Bazán

Contents

1. INTRODUCTION

1.1. Motivation

This study aims to experimentally analyse the rising movement of a bubble due to its interaction with solid vertical walls. The presence of such walls may cause complex changes in the bubble's trajectory by inducing a force that is determining for its position. In this case, Galileo and Bond numbers (*Ga* and *Bo* respectively) are to be considered, as well as the influence of a separation parameter S, as will be described later.

In previous researches, it has been noted that different vorticity generation mechanisms compete to determine the direction of this force. However, they have not been characterized in detail so far. Therefore, it would be of great interest to obtain global correlations that fit those findings.

The interest of this investigation resides in the multiple industrial applications of bubbles. For example: mineral purification by flotation, water treatment by aeration of chemical or biological reactors. They are also essential for several applications in pharmaceutical and biomedical industry (medicaments transportation) and food industry (e.g. carbonated drinks, mousse aeration), among many others [1]. These processes could be optimized if the path of the bubbles could be precisely predicted.

Consequently, this work addresses to extend the study of the effect of the presence of a vertical wall to regimes of rectilinear and planar zigzagging rising bubbles (those which happen for high values of *Ga* and low values of *Bo*) as well as three-dimensional spiral regimes (for high values of *Ga* and *Bo*). Thereby, the influence of the wall will be characterized for different regimes through the *Ga*-*Bo* plane.

1.2. Objectives

The main aim of this work is to identify and characterize the mechanisms that govern the movement of an individual bubble in presence of a close vertical wall.

For this reason, the study also intends to determine the influence of the vertical surface in the transitions between different regimes, considering *Ga* and *Bo* and the additional parameter S.

1.3. Previous research

1.3.1. Bubble formation

The bubble formation, or bubbling process can be described by a two-stage phenomenon: an expansion is followed by a collapse stage [1]. After expansion, the upwards buoyancy force overtakes the downwards surface tension force. At this moment, a neck appears in the vicinity of the nozzle on the bubble surface, the bubble equilibrium shape becomes unstable, and the dynamic collapse stage starts. In this phase, the neck accelerates radially inwards while it propagates downwards until it collapses, producing the release of the main bubble. This break-up phenomenon is commonly known as pinch-of [1].

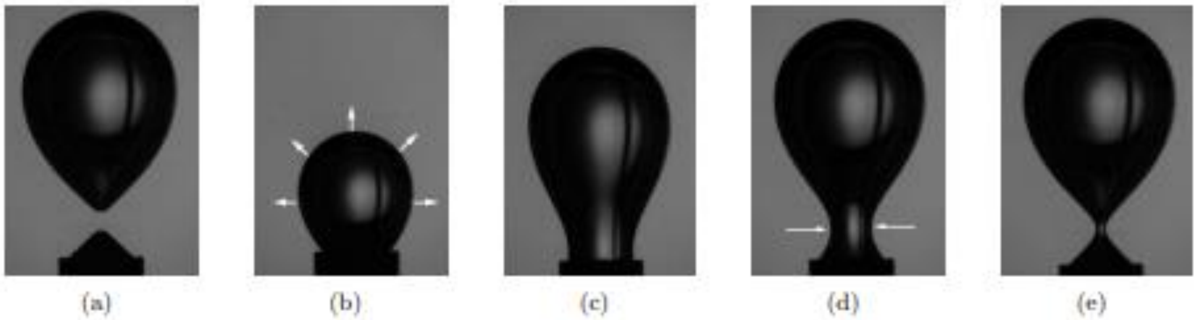

Figure 1.1: Temporal sequence of snapshots corresponding to a bubble growing quasi-statically from a vertical injector submerged in a pool of stagnant liquid. Images (a) – (c) show the expansion stage and (c) – (e), the collapse stage. Taken from **[1]**.

Depending on the initial conditions and control parameters, two different types of axisymmetric bubble break-up exist regarding the symmetry of the process with respect to a plane perpendicular to the centreline of the injector [2]: symmetric vs. asymmetric pinch-of. The bubbles recorded for this work experienced a symmetric break-up.

Another important variable regarding bubble formation is air flow rate (Q). Below a certain value, known as critical flow rate, the volumes of the bubbles at detachment are independent of Q or, in other words, bubbles are formed under quasi – static conditions [1]. This critical value was given by Oguz and Prosperetti [3] as $Q_c = \pi(16/3g^2)^{1/6}(\sigma R_i/\rho)^{5/6}$, where Q_c stands for the critical flow rate, g for gravity acceleration, R_i is the injector radius, σ is the surface tension of the fluid and ρ is its density.

These conditions mean that the bubble at detachment is determined by a balance between surface tension and buoyancy. The volume of this bubble, which is independent of the air flow rate Q, is commonly known as the *Fritz* volume and it follows the expression: $V_F = 2\pi\sigma R_i/(\rho g)$ [1].

1.3.2. Rise of bubble

After the bubble detaches from the injector, the rising stage starts. In the present work, we focus on this phase. During this stage, the bubbles rises with a certain path.

The fact that the path of a rising bubble in a still liquid stops following a straight line to switch to a zigzag or helical trajectory has been widely studied, although not fully understood yet [4].

It has been observed that different paths and wakes may happen and depend on the volume of the bubble, e.g. in clean water for bubbles with an equivalent radius larger than 81 mm bubbles no longer rise rectilinearly, but the path becomes a spiral or zigzag [4].

This problem can be entirely characterized using two parameters: Galileo number ($Ga = \rho g^{1/2} D^{3/2}/\mu$) and Bond number ($Bo = \rho g D^2/\sigma$). Eliminating D in both numbers, the Morton number is obtained ($Mo = Bo^3/Ga^4 = g\mu^4/\rho\sigma^3$) and it depends only on the liquid properties; hence, only two of these three parameters are enough [4].

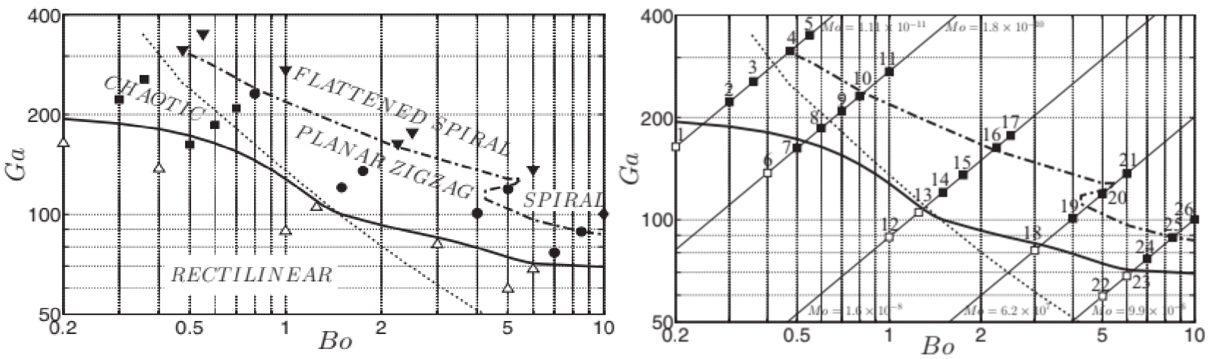

(a) (b)

Figure 1.2: Phase diagram summarizing the different styles of path observed in simulations. In (a) the cases are classified by type of path: (blank triangle stands for rectilinear, planar zigzag with a full circle; flattened spiral with inverted triangles, spiral (helical) with diamonds, and chaotic with squares). The three curves are identical to those in (b), which shows the simulated flow conditions corresponding to table 1.1. Taken from **[4]**.

Consequently, different behaviours of the bubbles can be seen depending on the values of Bo and Ga, defining different regimes in the Ga – Bo plane. Figure 1.2 shows the areas where the rectilinear path is stable, where it is unstable and a transition area where an incipient path instability exists. In the work by Cano-Lozano et al. [4] 26 numerical simulations where performed in these regimes, as seen in table 1.1.

Therefore, some of the cases analysed by them were duplicated in this experimental study, with the objective of contrasting the differences and similarities between the numerical and experimental work as well as between the case with or without the influence of the wall.

Case	Liquid	Mo	Bo	Ga	St	Path	Wake	Regime
1	water	1.11×10^{-11}	0.2	163.88		rectilinear	axisymmetric	rectilinear
2	water	1.11×10^{-11}	0.3	222.13		chaotic	2CRV aperiodic	chaotic
3	water	1.11×10^{-11}	0.36	255.28		chaotic	2CRV aperiodic	chaotic
4	water	1.11×10^{-11}	0.475	313.54	0.042	chaotic or elliptical spiral	2CRV aperiodic+SHV	transitional
5	water	1.11×10^{-11}	0.55	350.20	0.045	elliptical spiral → planar zigzag	2CRV 2R+SHV	FS → zigzagging
6	T00	1.8×10^{-10}	0.4	137.31		rectilinear	axisymmetric	rectilinear
7	T00	1.8×10^{-10}	0.5	162.34		chaotic	2CRV aperiodic	chaotic
8	T00	1.8×10^{-10}	0.6	186.12		chaotic	2CRV aperiodic	chaotic
9	T00	1.8×10^{-10}	0.7	208.93		chaotic	2CRV aperiodic	chaotic
10	T00	1.8×10^{-10}	0.8	230.94	0.054	planar zigzag	2CRV+SHV	zigzagging
11	T00	1.8×10^{-10}	1.0	273.01	0.060	elliptical spiral → planar zigzag	2CRV+SHV	FS → zigzagging
12	T02	1.6×10^{-8}	1.0	88.92		rectilinear	axisymmetric	rectilinear
13	T02	1.6×10^{-8}	1.25	105.11		rectilinear	axisymmetric	rectilinear
14	T02	1.6×10^{-8}	1.50	120.51	0.069	planar zigzag	2CRV 2R	zigzagging
15	T02	1.6×10^{-8}	1.75	135.3	0.073	planar zigzag	2CRV 2R	zigzagging
16	T02	1.6×10^{-8}	2.25	163.35	0.090	elliptical spiral → planar zigzag	2CRV 4R	FS → zigzagging
17	T02	1.6×10^{-8}	2.5	176.77	0.095	elliptical spiral → planar zigzag	2CRV 4R	FS → zigzagging
18	T05	6.2×10^{-7}	3.0	81.23		rectilinear	axisymmetric	rectilinear
19	T05	6.2×10^{-7}	4.0	100.8	0.108	planar zigzag	2CRV 2R	zigzagging
20	T05	6.2×10^{-7}	5.0	119.2	0.123	planar zigzag	2CRV 4R	zigzagging
21	T05	6.2×10^{-7}	6.0	136.6	0.138	elliptical spiral → planar zigzag	2CRV 4R	FS → zigzagging
22	T11	9.9×10^{-6}	5.0	59.61		rectilinear	axisymmetric	rectilinear
23	T11	9.9×10^{-6}	6.0	68.34		rectilinear	axisymmetric	rectilinear
24	T11	9.9×10^{-6}	7.0	76.72	0.120	planar zigzag	2CRV 2R	zigzagging
25	T11	9.9×10^{-6}	8.5	88.74	0.132	planar zigzag	2CRV 2R	zigzagging
26	T11	9.9×10^{-6}	10.0	100.25	0.136 → 0.174	planar zigzag → helix (spiral)	spiral	spiraling

Table 1.1: Characteristic properties of the 26 flow conditions considered in the study by Cano-Lozano et al. **[4]**.

Another aspect worth mentioning for isolated rising bubbles is their rising velocity, hence it has been found that the bubble experiences different phases while it rises. First, when the bubble detaches from the injector, its shape is essentially spherical and it rapidly accelerates in the vertical direction. After some time it becomes oblate, hence it displaces more fluid and the drag force increases. Finally, balance between buoyancy and drag forces results in a quasi-terminal rise velocity that remains constant indefinitely [4].

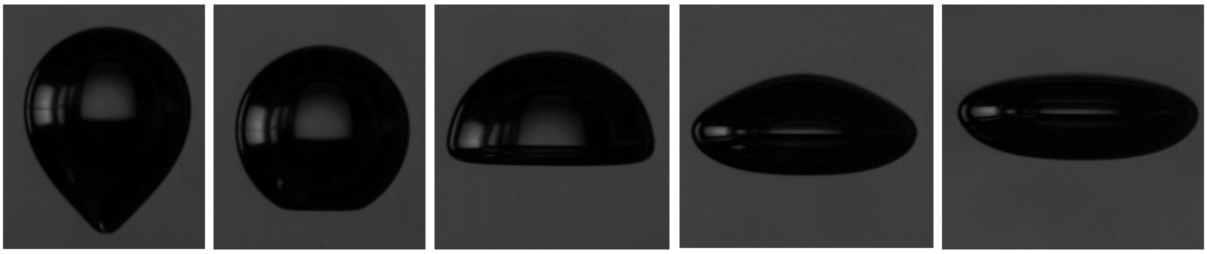

(a) (b) (c) (d) (e)

Figure 1.3: Time evolution of the shape of a bubble after detachment. Figures (a) and (b) show a nearly spherical shape while in (c) to (e) the bubble tends to become oblate.

1.3.3. Wall – bubble interaction

The problem involving the effect that a vertical wall causes in the path of an isolated bubble has been also studied both numerically and experimentally.

The case of a rising oscillating zigzagging bubble close to a vertical wall was studied by Lee and Park [5]. Their findings concluded that if the bubble collides with the wall, the bubble migrates away from the wall very fast to later quickly slow down moving back towards the wall. This change of direction occurs because as the bubble moves away from the wall, the vortex-induced force becomes more influential than the inertial force (the latter becomes smaller due to viscous dissipation through the wake-wall interaction); thus, the bubble decelerates and changes its direction [6]. Figure 1.4 shows that de Vries et al. [7] reached similar findings.

However, much smaller wall effects were found for the case without collision (bubble-wall distance of 1.9 times the bubble diameter).

Furthermore, Lee and Park [5] found that the wall induces more complex behaviour by cause of increased vorticity or boundary-layer like secondary flow structures. The horizontal movement of the bubble, which is caused due to surface energy is reduced in amplitude because of the wall interference causing energy waste.

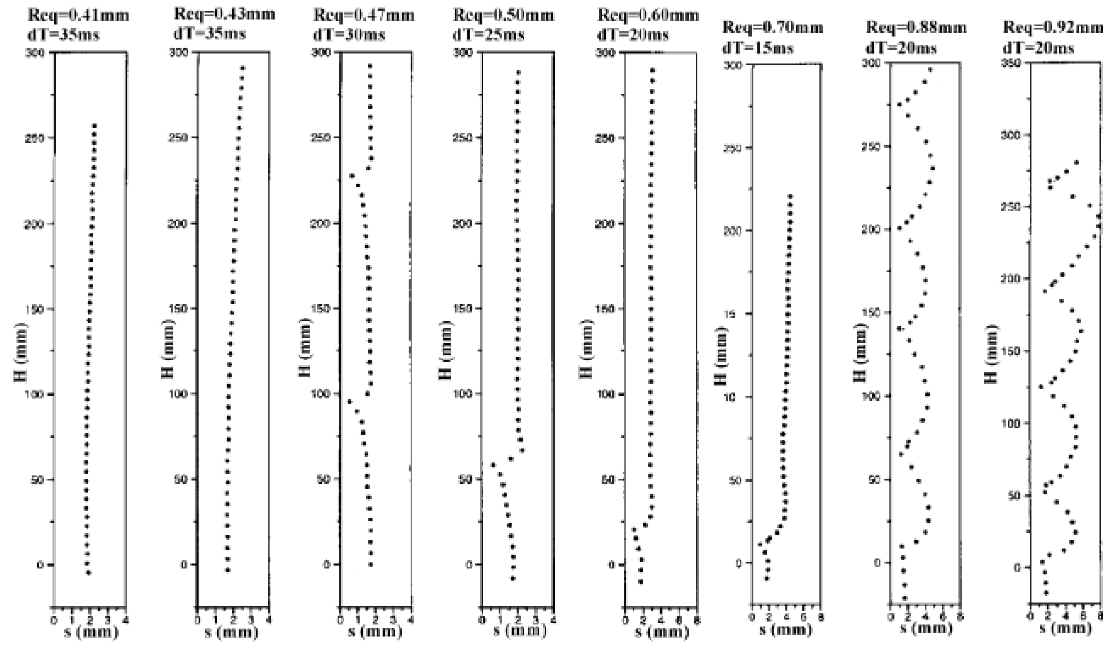

Figure 1.4: Experimentally determined trajectories of different sizes as they interact with a vertical wall. In all cases the initial separation s = 1.57 mm. Taken from **[7]**.

1.3.4. Image processing

Digital imaging is a non-intrusive method and does not require direct contact with the flow field, thus can achieve a high spatial and temporal resolution. With the major development of digital imaging technique in recent years, image processing combined with high speed cameras has become an attractive technique for its capability in obtaining high spatial and temporal resolution bubbly flow data [8].

Concerning bubble recording, the most typical imaging system implies large bubbles being back-lit by a diffuse source.

According to Bongiovanni et al. [9], this set – up is useful because some of the rays reach the lens of the camera directly without touching the bubble, forming the background illumination and thus leaving a dark disc which is the bubble shadow. Besides, doubly refracted rays produce a clear spot in the centre of the bubble. The spot radius depends on the size and distance of the source, and will be maximum for an infinite source. The reflected rays also form a bright ring inside the bubble shadow. The image of a spherical bubble has been found to be a dark ring on a clear background.

The brightness of the external ring due to reflected rays is very close to the background brightness and so cannot be distinguished from it. Due to this, the volume of gas may be underestimated, typically, the error made on the volume measurement will exceed 5% when a very large light source is utilized or when the bubble is very close to the source [9].

After getting these bubble images, post-processing will consist on extracting the bubble contour from its background. Fu and Liu [8] assure brightness correction and noise reduction are critical to provide a correct edge detection. Subtracting the background and the average image intensities, part of the noise can be removed. A global threshold is then used to convert the grey scale image to binary image. The Canny edge detector is used to acquire the outer and inner boundaries of bubbles for further processing [8].

The mentioned threshold should be carefully selected. N. Otsu [10] derived a method based on integration of the grey-level histogram of an image. This is a global property of the image, unlike differentiation, which is used in other methods such as valley detection and is a local property.

This method consists on defining the probability of a pixel with a certain grey level being part of the "class" background or the "class" object by a certain threshold [10]. Then, in order to evaluate the "goodness" of the threshold discriminant criterion measures are introduced. Thus, the problem is reduced to an optimization problem to search for a threshold that maximizes one of the criterion measures. This standpoint is motivated by a conjecture that well thresholded classes would be separated in grey levels, and conversely, a threshold giving the best separation of classes in grey levels would be the best threshold [10].

These characteristics and the utilization of integration make Otsu method quite general, covering a wide scope of unsupervised decision procedure and opting for one automatic, stable, optimal threshold for each image [10]. Otsu threshold selecting method was utilized for most images in this work.

2. DESCRIPTION OF THE PROBLEM

The problem of an isolated rising bubble in the proximity of a solid vertical wall is described as shows figure 2.1.b.

As describes Cano- Lozano et al. [4], the problem of an isolated rising bubble can be described using three dimensionless parameters. Adding variable s, which stands for the distance between the bubble centroid and the wall surface, the resulting problem variables are the ones shown in figure 2.1.a: fluid properties, bubble diameter, gravity, rise velocity and distance to the wall.

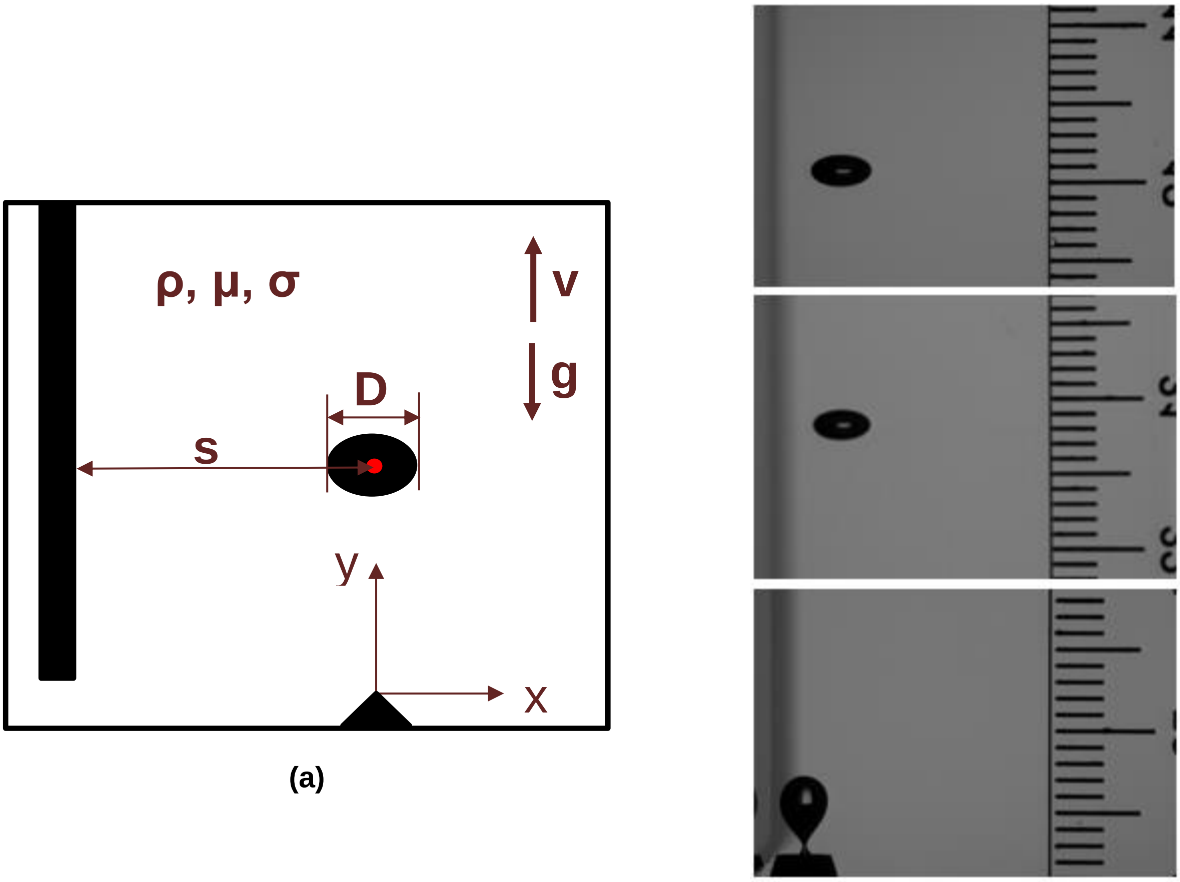

(a) (b)

Figure 2.1: (a) Scheme of the variables of the problem, where ρ stands for fluid density; σ, for fluid surface tension; μ, for fluid viscosity; g is gravity acceleration; s is the distance between the surface of the wall and the bubble centroid; D is the equivalent diameter of the bubble and v, which is the main unknown, stands for the rising terminal velocity of the bubble. The coordinates' origin is on the centre of the injector. (b) Sequence of pictures of the experiments developed at three different levels of the tank (lowest, medium, and highest).

Note that the characteristic length that will be used to define the dimensionless parameters is the equivalent bubble diameter. Bubbles are not perfect spheres; hence, this diameter is defined as the diameter of a sphere of same volume as the bubble.

Evaluating Buckingham Π theorem for these variables, it is found that four dimensionless numbers are enough to define the problem:

	v	ρ	μ	σ	g	D	s
M	0	1	1	1	0	0	0
L	1	-3	-1	0	1	1	1
T	-1	0	-1	-2	-2	0	0

Table 2.1: Dimensions of the problem variables. M stands for mass dimensions; L, for length dimensions and T, for time dimensions. The content describes the exponentss of each variable's dimensions.

The base for the dimensionless number will be compound of three of these variables, namely density (ρ), gravity (g) and bubble equivalent diameter (D). Hence, at least one fluid property, one flow property and one bubble property will be present in every parameter. Then, the remaining variables is combined with the base in order to obtain a dimensionless number for each of them. The obtained dimensionless parameters that fully describe the problem are defined as shown by the following equations:

$$\Pi_0 = \frac{v}{\sqrt{gD}} \qquad \Pi_1 = \frac{\sigma}{\rho g D^2} \qquad \Pi_2 = \frac{\mu}{\rho\sqrt{gD^3}} \qquad \Pi_3 = \frac{s}{D}$$

$$\Pi_0 = F(\Pi_0, \Pi_0, \Pi_0); \quad \frac{v}{\sqrt{gD}} = F\left(\frac{\sigma}{\rho g D^2}, \frac{\mu}{\rho\sqrt{gD^3}}, \frac{s}{D}\right)$$

Dimensionless numbers Π_1 and Π_2 stand for the inverse of Bond and Galileo numbers respectively. The first weighs buoyancy force vs. surface tension effects; while the latter evaluates the importance of weight vs. viscosity effects [11]. As explained by Cano-Lozano et al. [4] an additional parameter should be added in order to define the characteristics of the fluid (Morton number). It can be obtained by combination of Bond and Galileo numbers when D is eliminated.

Furthermore, using Reynolds number would be practical for analysis. Hence, it can substitute dimensionless number Π_4 (Froude number) by combining it with Π_2 (Galileo number). The resulting parameters, which entirely describe the problem of a rising bubble close to a vertical wall, are described as follows:

$$\mathrm{Bo} = \frac{\rho g D^2}{\sigma} \qquad \mathrm{Ga} = \frac{\rho D\sqrt{gD}}{\mu} \qquad \mathrm{Mo} = \frac{Bo^3}{Ga^4} = \frac{g\mu^4}{\rho\sigma^3} \qquad \mathrm{S} = \frac{s}{D} \qquad Re = Ga \cdot Fr = \frac{\rho v D}{\mu}$$

$$Re = F(Bo, Ga, S)$$

3. EXPERIMENTS

3.1. Experimental set-up

The experiments were developed in a hexahedral tank of 60x15x15 cm^3. The vertical dimension of the tank was designed much larger than the rest so that the liquid column was high enough for the bubble to develop its path and terminal velocity.

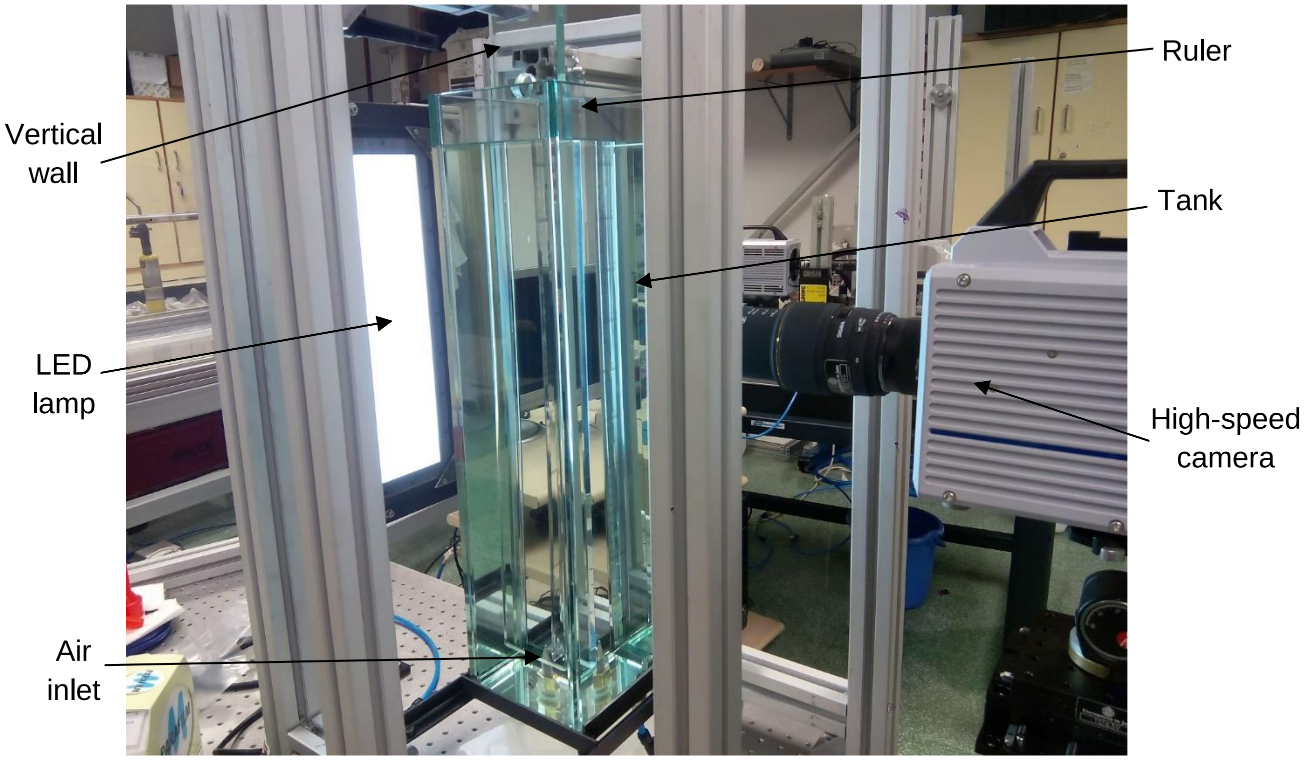

Figure 3.1: Picture of the equipment used to run the experiments.

Moreover, the tank was made of glass. This material was chosen because of its resistance to alcohol as a means of cleaning. This was necessary because elimination of surfactants was vital for the experiment, as their presence may affect the gas-liquid interface, changing the shear-free boundary condition satisfied by the liquid into a no-slip one at least on a part of the interface, therefore modifying the flow structure past the bubble, hence the threshold of the instability [12] - [13]. Surfactants are not that determining when using nonpolar fluids, but they are for water based mixtures.

It was also essential that the installation allowed us to easily change the control parameters, especially the distance between the wall and the bubble centroid (s). Therefore, the vertical wall was installed as a rack and pinion mechanism so that the distance to the nozzle was variable.

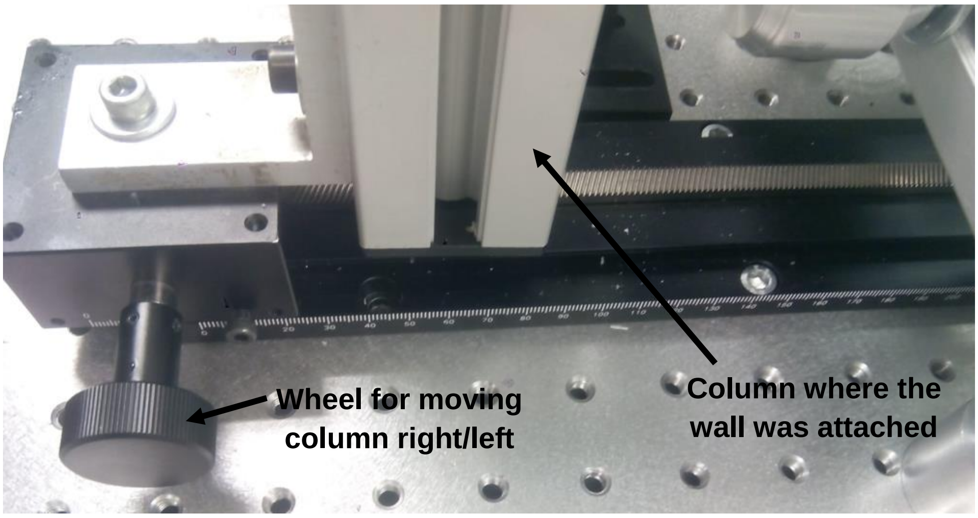

Figure 3.2: Wall movement mechanism.

In order to relate the bubble vertical position to a reference, a ruler was hanged over the tank. A small mass was put on its low end to prevent bending. The ruler was also used for images resolution calculation.

Figure 3.3: Ruler used for positioning and calculation of resolution.

The nozzle for the air inlet was located at the centre of the bottom wall in order to assure that the influence of the vertical surface is more determining than that of the tank walls, as they were far enough to neglect their effects. The inlet diameter was determined based on the numerical simulations by Cano-Lozano et al. [4].

Case	Liquid	Mo	Bo	Ga	St	Path	Wake	Regime
22	T11	9.9×10^{-6}	5.0	59.61		rectilinear	axisymmetric	rectilinear
23	T11	9.9×10^{-6}	6.0	68.34		rectilinear	axisymmetric	rectilinear
24	T11	9.9×10^{-6}	7.0	76.72	0.120	planar zigzag	2CRV 2R	zigzagging
25	T11	9.9×10^{-6}	8.5	88.74	0.132	planar zigzag	2CRV 2R	zigzagging
26	T11	9.9×10^{-6}	10.0	100.25	$0.136 \rightarrow 0.174$	planar zigzag → helix (spiral)	spiral	spiraling

Table 3.1: Characteristic properties of the selected flow conditions considered in the study by Cano-Lozano et al. **[4]**.

For the stable regime the selected diameter was 2.35 mm (see bubbles 22, 23 in 3.1); while for the transition regime diameters of 7.40, 10.00 and 12.60 mm were chosen (bubbles 24, 25, 26 in table 3.1). However, due to the high time-consuming nature of the experiments only the 10 mm diameter was tested for the transition regime.

(a) (b)

Figure 3.4: Nozzles used for air inlet. Figure (a) shows the 2.35 mm nozzle while (b) shows the surface orifice that was treated in order to provide a 10 mm diameter for the inlet, as will be explained later.

Assuming quasi-static conditions, the diameters of the nozzles could be calculated using *Fritz* volume hypothesis. This consists on evaluating an equilibrium between surface tension and gravitational forces and considering the bubble is a perfect sphere:

$$\pi \cdot d \cdot \sigma = \rho \cdot g \cdot V; \qquad V = \frac{\pi}{6} \cdot D^3 = \frac{\pi \cdot d \cdot \sigma}{\rho \cdot g}; \qquad d = \sqrt[3]{\frac{\rho \cdot g \cdot D^3}{6 \cdot \sigma}}$$

Where d is the diameter of the injector, D is the diameter of the bubble, g is gravity acceleration and ρ and σ are the fluid density and surface tension respectively.

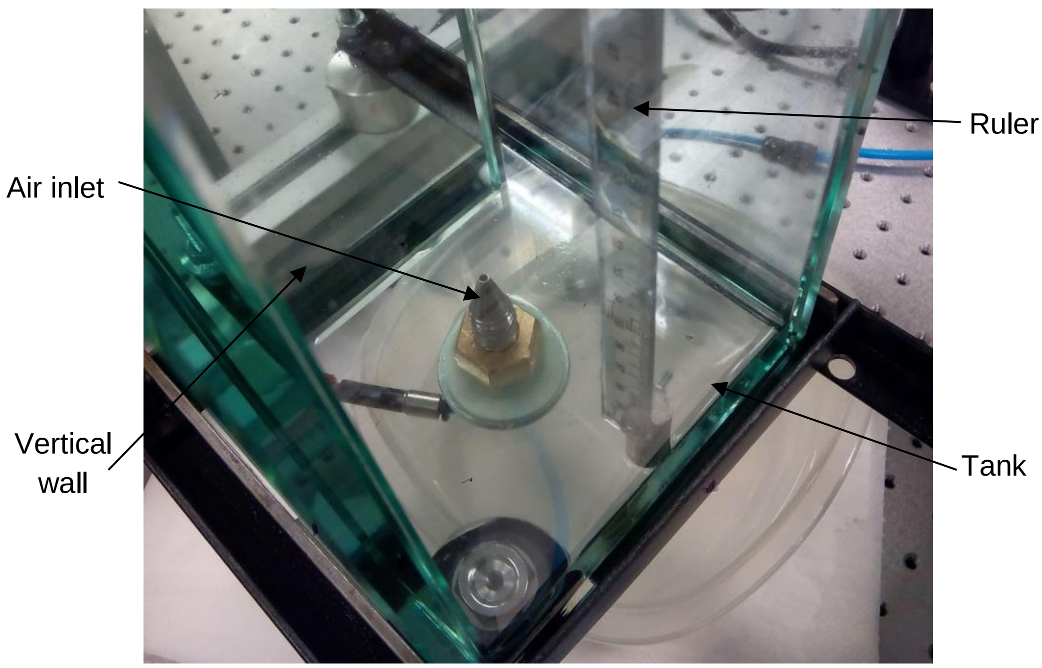

Figure 3.5: Picture of the bottom of the tank, showing all its components and the 2.35 mm nozzle installed.

In order to achieve the largest bubble diameters, surface orifices where covered with a hydrophobic coat (Rustoleum NeverWet). This substance prevents water form covering the orifice so that air can fill all the treated area; hence a water based mixture had to be used as work fluid for these cases.

(a) (b) (c) (d) (e)

Figure 3.6: Evolution of the formation of a bubble on a surface orifice treated with Rustoleum NeverWet. Figures (a) – (c) show how air covers all the treated surface. Figures (d) and (e) show that when the bubble becomes too large, the contact angle increases and the collapse stage begins.

3.1.1. Fluids selection

With the fluid properties the experiments are now entirely characterized. For the bubbles in the stable regime, the same fluid Cano-Lozano et al. [4] used for simulations was utilized in the experiments with the aim to compare with their findings. Given its properties [14], the nozzle diameter previously pointed was calculated assuming *Fritz* volume hypothesis.

Liquid	ρ (kg/m^3)	μ (mPa s)	σ (mN/m)	$Mo = g\mu^4/(\rho\sigma^3)$
Water	1000	1.00	72.86	2.5×10^{-11}
DMS-T00	761	0.49	15.9	1.8×10^{-10}
DMS-T02	873	1.75	18.7	1.6×10^{-8}
DMS-T05	918	4.59	19.7	6.2×10^{-7}
DMS-T11	935	9.35	20.1	9.9×10^{-6}

Table 3.2: Properties of the liquis used in the experiments by Zenit and Magnaudet **[14]**: ρ is the density, μ the dynamic viscosity, and σ the surface tension. The properties of pure water are also shown for reference.

However, for the bubbles in the transition regime this fluid was not valid, as the calculated nozzle diameter (by *Fritz* volume hypothesis) was too large, surpassing the surface tension limit. This would have meant that the air would not have come out of the nozzle, but the fluid would have come into the air line.

As explained in the previous section, the largest diameters were obtained using a hydrophobic coat. Silicon oil is not repelled by hydrophobic substances; consequently, a different fluid was chosen for this regime; thus, a water – glycerol mixture was used instead. In particular, water – glycerol mixture would provide the required value of Morton number.

Several data for the fluid properties of water – glycerol mixtures for variable concentration and temperature were provided by Dow Corning and Miner and Dalton [15]; as shown in figure 3.7. For the fixed Morton number and laboratory temperature (≈ 22.5 ºC), an ideal concentration was interpolated so that it would provide the cases studied by Cano-Lozano et al. [4]. The target viscosity resulted 24.4 cP and the concentration should be 73.05% in weight of glycerol for that purpose.

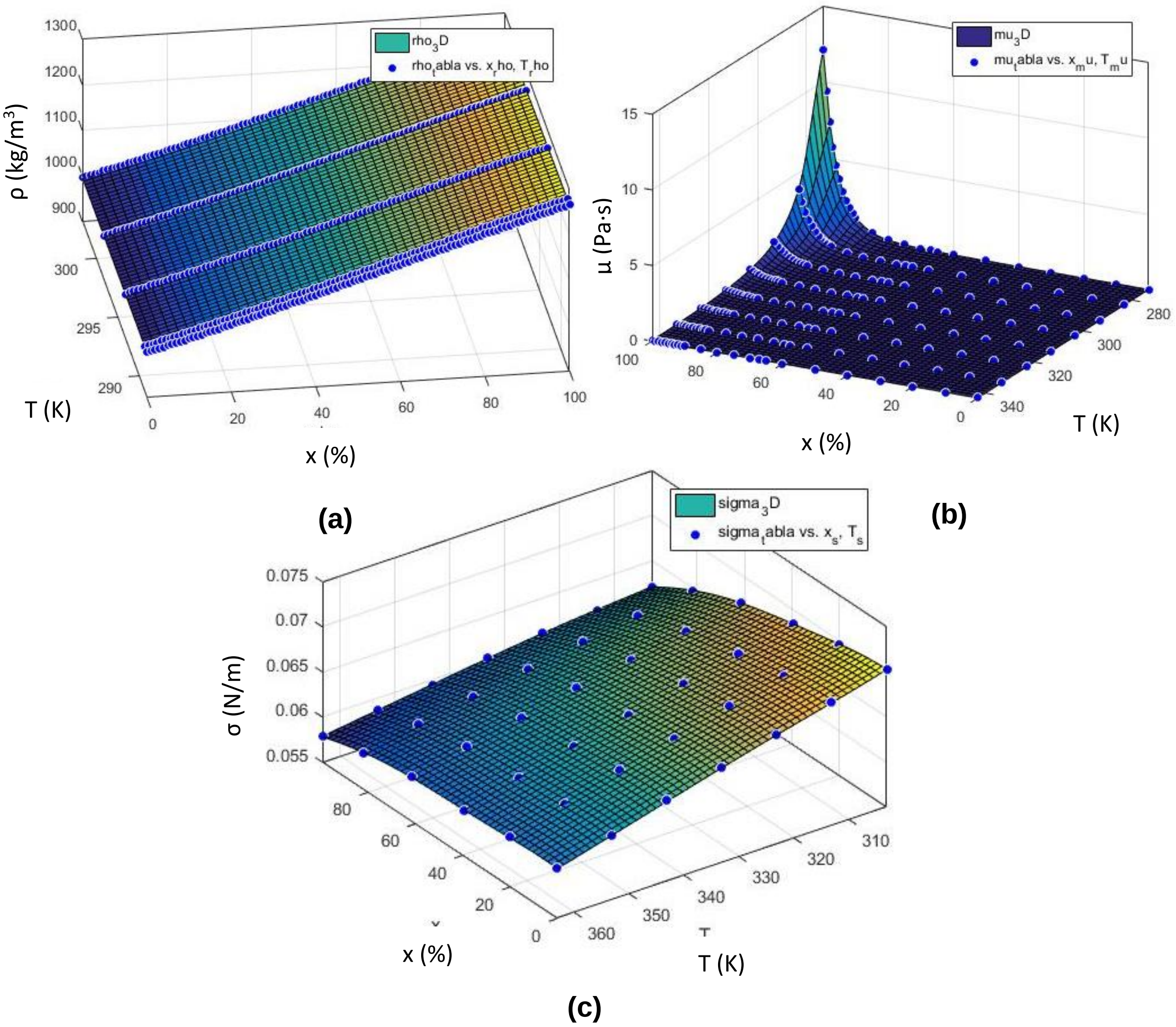

Figure 3.7: Interpolation of data from Dow Corning and **[15]** used to calculate (a) density, ρ; (b) dynamic viscosity, μ; and (c) surface tension, σ for fixed values of Mo, Bo, Ga and temperature (T) and variable concentration (x).

Considering Ga and Bo numbers and the concentration, the bubble equivalent diameter was calculated. Finally, the nozzle diameters previously marked were derived using *Fritz* volume hypothesis ($d = (\rho\ g\ D^3 / (6\ \sigma))^{1/3}$).

Bubble	Ga	Bo	D (mm)	d (mm)
24	76.72	7.0	6.34	7.39
25	88.74	8.5	6.98	9.89
26	100.25	10.0	7.57	12.62

Table 3.3: Bubble target equivalent diameters (D) and nozzle diameters (d) for the experiments in the transition regime.

While running the experiments, the laboratory conditions (temperature) changed. Hence, viscosity was also modified and different values of Mo, Bo and Ga characterized the experiments:

	T (ºC)	μ (cP)	Mo	Bo	Ga
Target conditions	22.5	24.40	9.90 E-06	8.5	88.74
Laboratory conditions	24.3	26.32	12.94 E-06	6.69	69.38

Table 3.4: Parameters of the problem that chaged due to a temperature rise in the laboratory where the experiments were developed.

3.2. High-speed-images obtention

Concerning experiments recording, several elements had to be added to the installation.

A high speed camera (FASTCAM SA1.1) was installed parallel to the tank in order to capture images of the rising bubbles. Behind the tank, a LED array lamp was needed in order to provide enough light for the camera to record at speeds between 1000 and 3000 fps. These conditions provided resolutions between 20 and 44 μm/pixel.

(a) **(b)**

Figure 3.8: FASTCAM SA1.1 camera with Sigma AF- MF ZOOM lens 105 mm F2.8 EX DG MACRO.

A Sigma AF- MF ZOOM lens 105 mm F2.8 EX DG MACRO was chosen for the camera. This model was selected because it provided enough focusing depth so that the captured images remained focused even though the bubbles moved away from the initially focused position.

The camera was installed on a Manfrotto 475 tripod as a means of support and in order to control the vertical movement of the camera. Below the camera, a Manfrotto 405 ball joint was added to allow for small angles in every direction, which was vital for levelling the camera before recording. Finally, a two-axis translation stage was inserted below the ball joint to allow for movements of ± 25 mm in the x direction (for placing the bubble trajectory in the camera plane) and the z direction (making focusing easier).

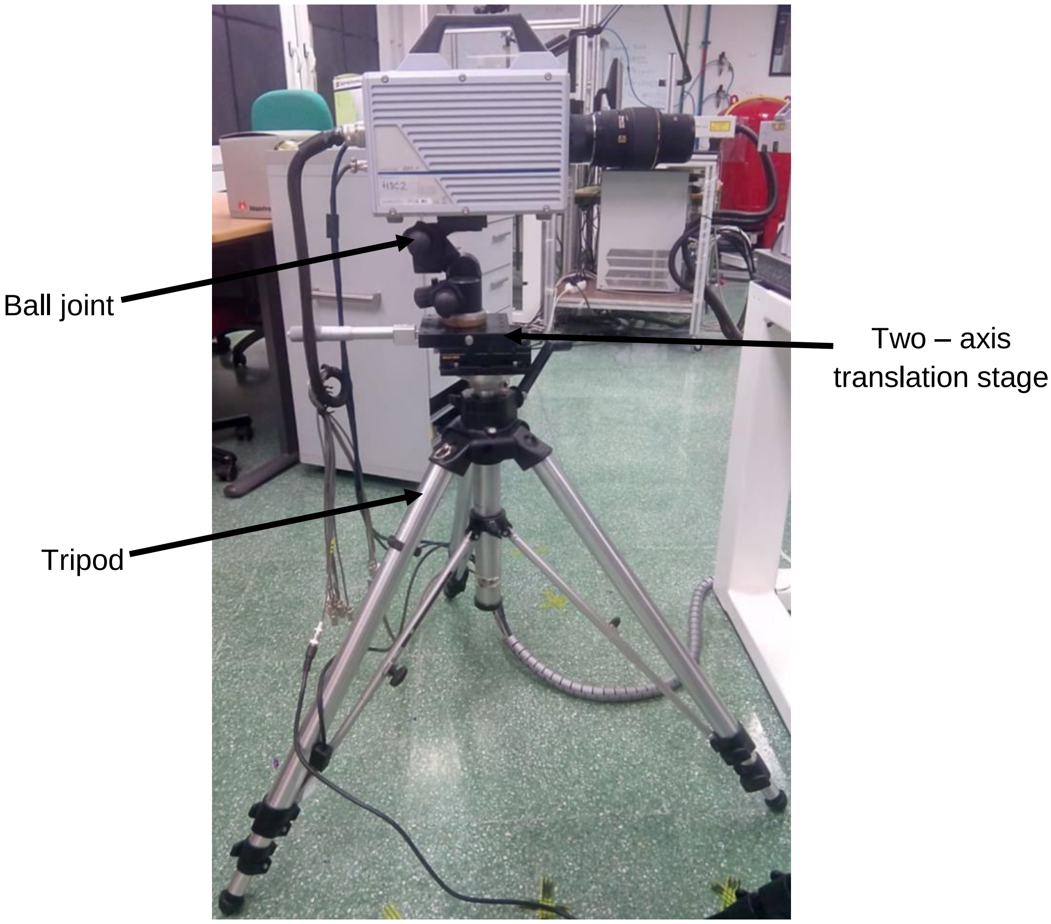

Figure 3.9: Camera support compound of Manfrotto 475 tripod, Manfrotto 405 ball joint and two-axis translation stage

For the zigzag regime, a second camera with all the mentioned additional components and another LED lamp was placed perpendicularly to the first ones in order to record the movements of the bubbles in both planes. To assure that both cameras recorded the same section of the tank, a laser level was installed. It reached both cameras' lenses so that height differences could be perceived and fixed. This was essential because cameras were synchronized so that they recorded at the same time, so misalignments in the height of the cameras would lead to recordings where the bubbles would not have appear.

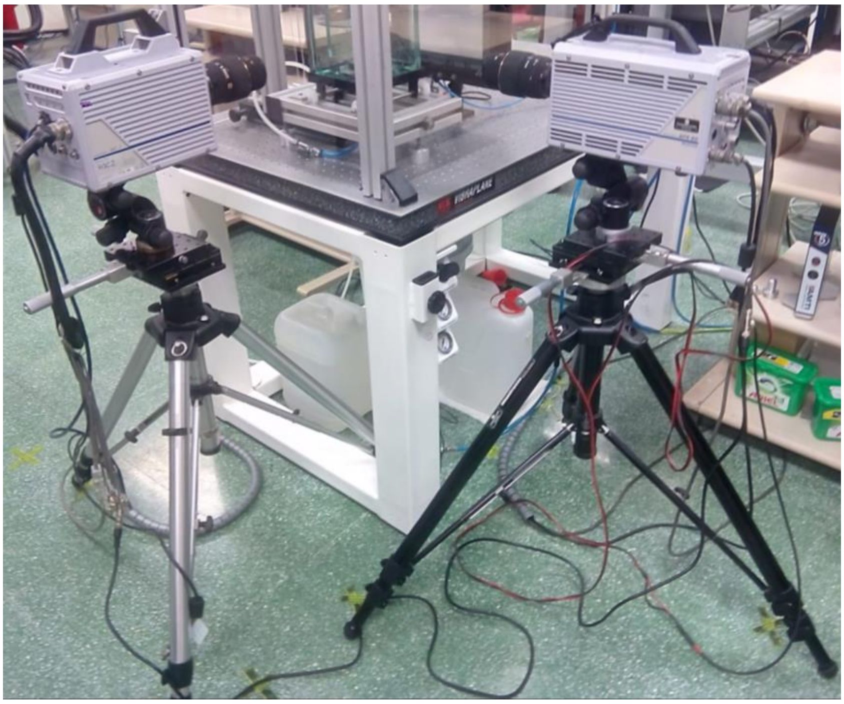

Figure 3.10: Set – up with two synchronised cameras.

The images acquisition consisted on the recording of the complete height of the tank divided into sections that the cameras could capture. Thus, 17 to 24 videos were recorded per camera for each trajectory.

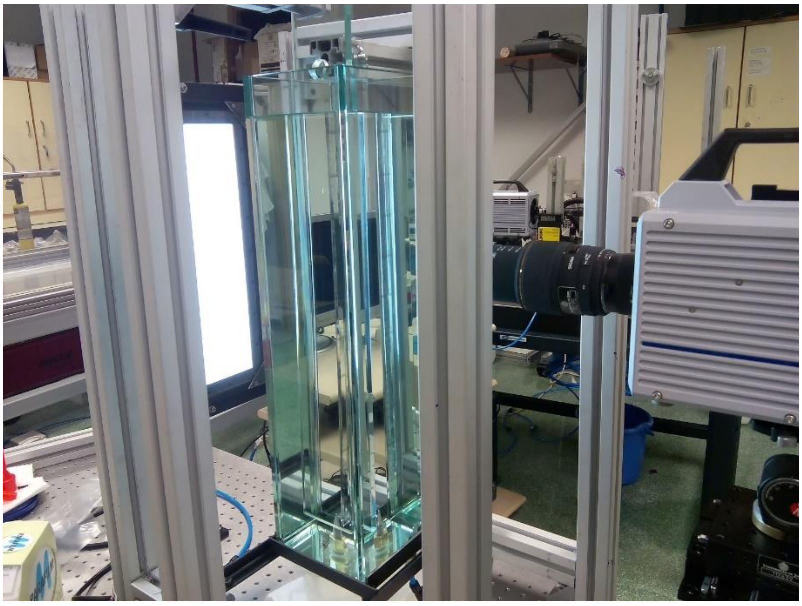

Figure 3.11: Set – up while performing a recording.

The rising time was also a determining variable, therefore videos should start at the instant when the bubble detached from the nozzle. The system developed to assure this consisted on a photodiode sensor that sent a signal to the cameras (via an Arduino controller) so that recording began when the bubble passed in front of the sensor.

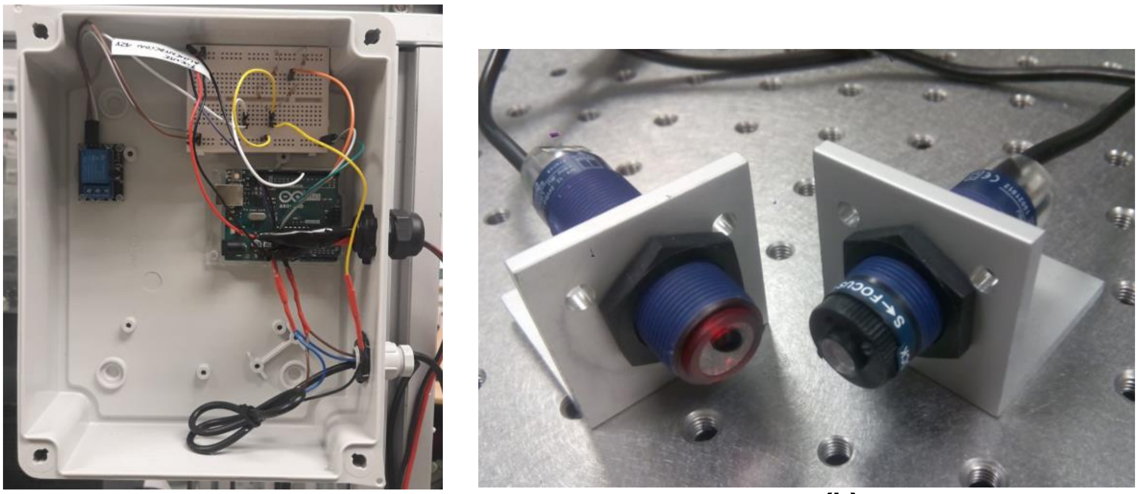

(a) **(b)**

Figure 3.12: Control system used to activate cameras. Figure (a) shows the Arduino circuit and (b) shows the photodiode sensor.

4. IMAGE PROCESSING

The videos were classified attending the value of S and the vertical position were each video was recorded. They were processed using three different routines self-developed on MATLAB.

The first routine's objective was to obtain the bubbles' properties, namely contour, centroid, section and volume.

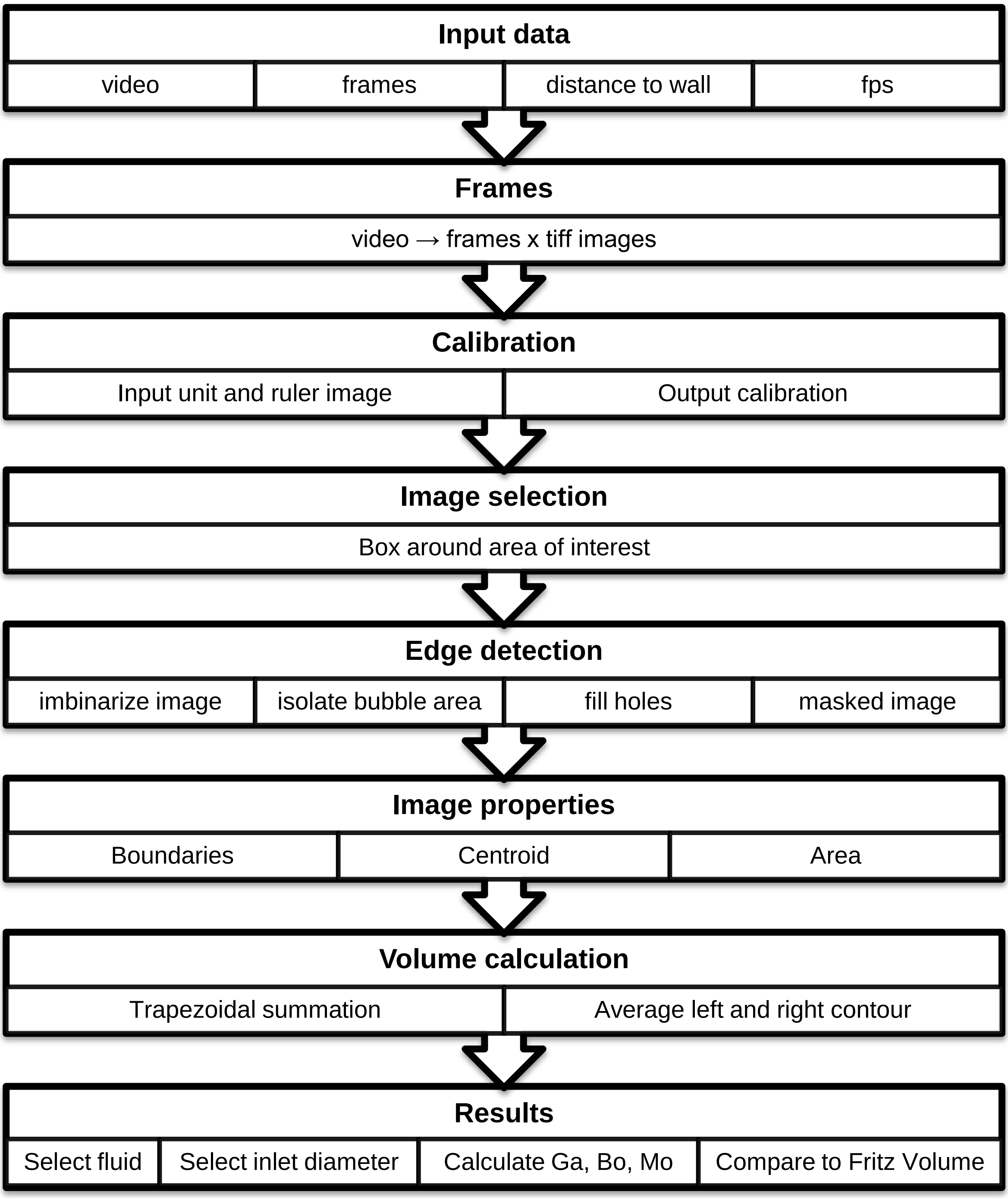

Figure 4.1: Block diagram describing the MATLAB routine realized to obtain bubbles' properties.

The procedure was the one explained in figure 4.1. Given S and the video parameters (filename, number of frames, velocity of image acquisition), the videos were separated into individual images that could be easily analysed.

For every video a photograph of the ruler in the tank was taken as a means of calibration. This calibration was obtained as an average of 10 measures performed by hand using MATLAB graphic tools. Following the same method, the area of the image where the movement of the bubble happens was selected for it to be analysed.

In order to detect the edges of the bubble, the image was imbinarized and the dark areas (bubble included) were turned white in the original image. Then the clear spot at the centre (caused by doubly reflected rays as for Bongiovanni et al. [9]) was filled and the bright area was detected (figure 4.2).

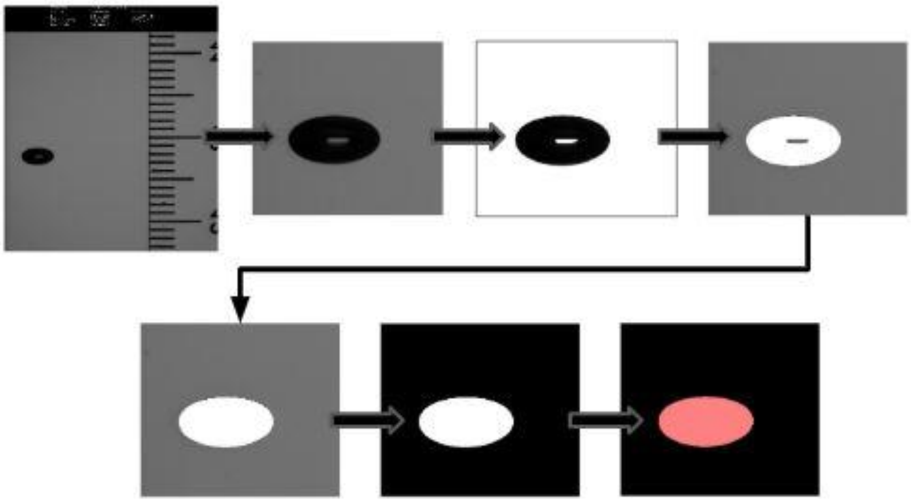

Figure 4.2: Example of the steps followed in the routine in order to separate the bubble from its background and detect its area and boundaries.

With the help of MATLAB Image Segmenting Tools, the properties of this area were calculated: boundaries, centroid and section.

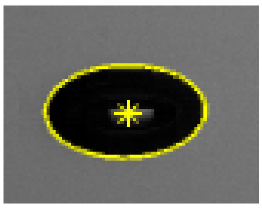

Figure 4.3: Example of edge and centroid detection.

Figure 4.4 shows an error in the edge detection step. It is worth mentioning that the selection of the parameters for boundaries identification was difficult due to the proximity to the wall because its shadow affected the results if the threshold was not carefully specified. In most cases the threshold was automatically selected as for N. Otsu [10], although sometimes it had to be reduced to avoid this.

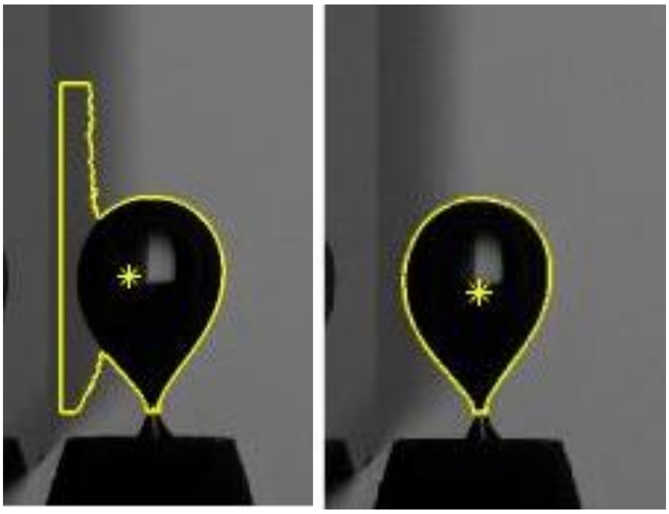

Figure 4.4: Example of error in edge detection due to wrong threshold selection. The wall creates with its shadow a dark area that a high threshold cannot separate from the bubble.

Bubbles were supposed axisymmetric, hence the volume was calculated as the revolution of the area within the boundaries in 2π radians. This area was calculated as the sum of infinitesimal trapezoidal sections in the vertical direction. Applying the calibration, the results were obtained in millimetres.

Eventually, given the fluid properties and the nozzle diameter, the *Fritz* volume could be calculated and compared to that obtained from image processing (as well as the dimensionless numbers describing the experiments).

The second routine aimed to show the trajectory of the bubbles along the entire height of the tank.

The individual videos could only cover a limited height of 2.5 to 3 cm, thus several videos were necessary to complete a whole trajectory. Furthermore, the camera positions were selected so that each one overlapped with the following, assuring a full coverage of the trajectory. Because of this, 15 to 24 videos had to be recorded and analysed for each value of S.

These videos were aligned in order to compound the trajectories as figure 4.5 explains.

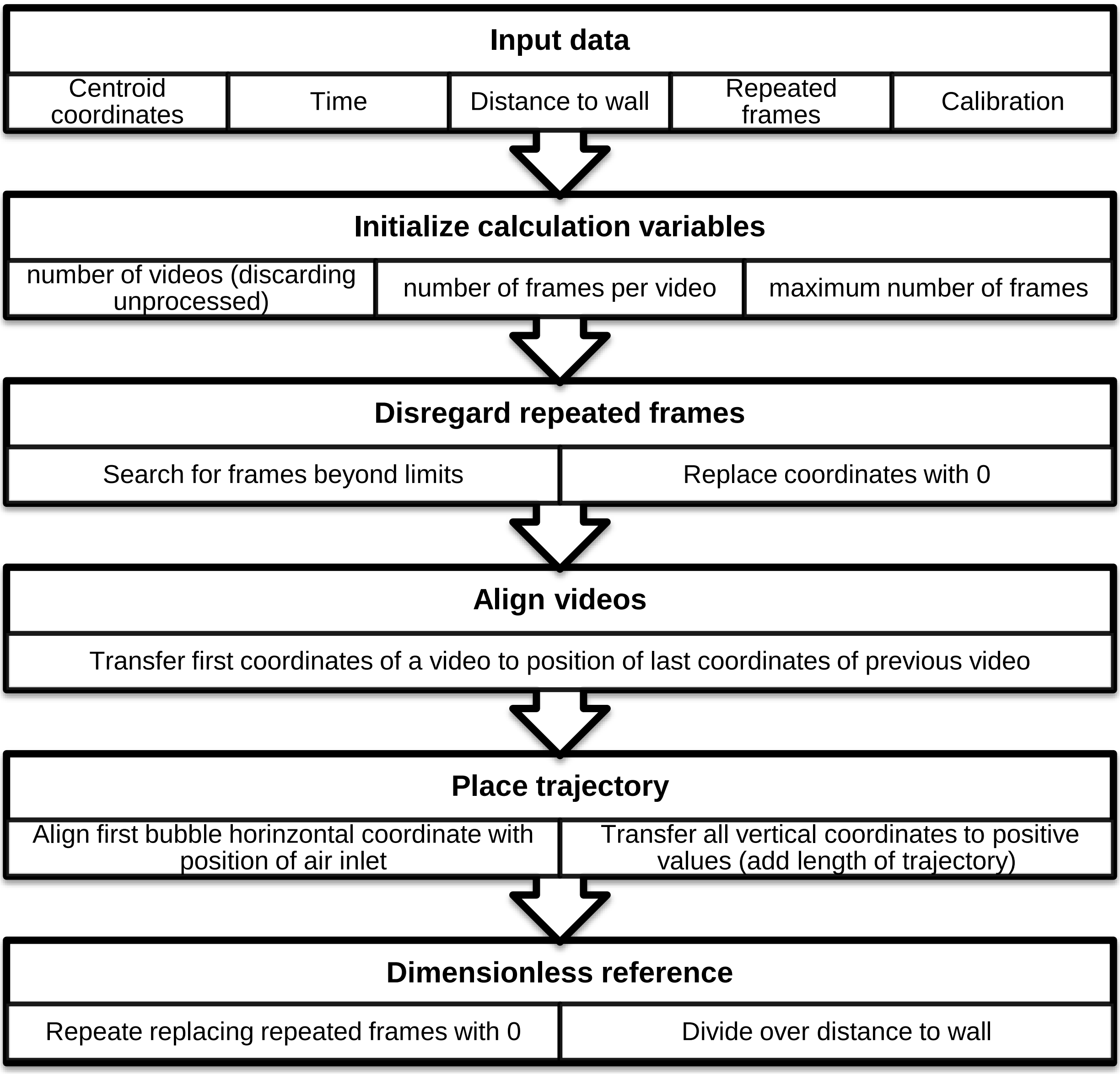

Figure 4.5: Block diagram describing the MATLAB routine realized to obtain bubbles' trajectories.

Firstly, the overlaps between videos were obtained and initialized as well as the calibrations, centroids' coordinates and time values; which were outputs from the previous routine.

Those frames whose centroid coordinates are beyond the limits marked by the overlapped sections are neglected. After that, the remaining frames' coordinates (both horizontal and vertical) are transferred so that the first point of a video coincides with the last point of the previous one. It should be remarked that even though it may appear that the horizontal coordinates must coincide among different videos. This was not the case due to small oscillations when the camera was moved vertically, which were probably caused by the weight of the camera and the existence of looseness in the mast of the tripod.

To conclude, the trajectories were translated to the coordinates' origin and made dimensionless by dividing over the bubble diameter. Thus, making the resulting graphs comparable to other cases.

The last routine was extremely related to the second one. It consisted on the calculation of the terminal velocity of the bubbles.

In order to obtain it, the alignment of the time values of consequent videos was necessary. After that, as is shown in figure 4.6, a centred differentiation of trajectory over time is performed.

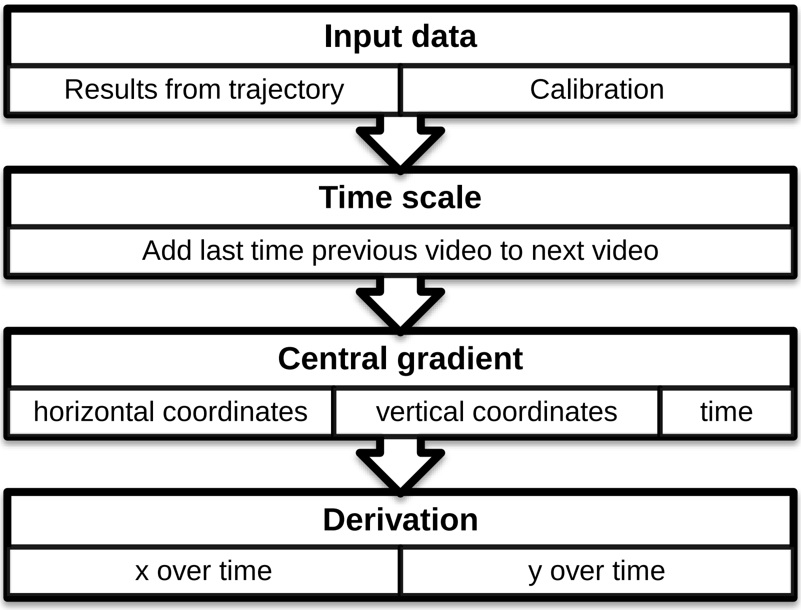

Figure 4.6: Block diagram describing the MATLAB routine realized to obtain bubble's velocity.

5. RESULTS

5.1. Initial bubble volume

The first result that can be derived from processing the images is the initial volume of the generated bubble. This stands for the validation of the *Fritz* volume hypothesis, and therefore, the quasi-static regime, used along the work to set the experiment parameters.

In table 5.1 the results from the experiments for the dimensionless numbers and the volume of the bubbles after detaching form the injector are shown. In the transition regime, the values of the dimensionless numbers were calculated for the target mixture (22.5º C, 24.4 cP); for comparison, the real values (24.3º C, 26.32 cP) are contained in the following table. This will not affect the volume.

STABLE REGIME				TRANSITION REGIME			
Volume (mm^3)	Bo	Ga	Mo	Volume (mm^3)	Bo	Ga	Mo
13.43	3.97	50.17	9.87E-06	175.79	8.44	88.30	9.90E-06
13.51	3.99	50.32	9.87E-06	173.68	8.38	87.77	9.90E-06
13.66	4.01	50.59	9.87E-06	180.07	8.58	89.37	9.90E-06
13.89	4.06	51.01	9.87E-06	180.74	8.60	89.54	9.90E-06
14.14	4.11	51.47	9.87E-06	184.94	8.74	90.57	9.90E-06
14.72	4.22	52.51	9.87E-06	166.31	8.14	85.89	9.90E-06
14.78	4.23	52.63	9.87E-06	159.75	7.92	84.18	9.90E-06
15.17	4.30	53.31	9.87E-06	180.55	8.60	89.49	9.90E-06
15.79	4.42	54.39	9.87E-06	173.58	8.37	87.75	9.90E-06
16.24	4.50	55.15	9.87E-06	197.61	9.13	93.62	9.90E-06
16.28	4.51	55.22	9.87E-06	182.44	8.66	89.96	9.90E-06
16.34	4.52	55.33	9.87E-06	164.35	8.07	85.38	9.90E-06

Table 5.1: Volume after detachment and dimensionless numbers of many bubbles for calculation of average.

Volume (mm^3)	Bo	Ga	Mo
175.79	6.63	68.90	12.94 E-06
173.68	6.58	68.48	12.94 E-06
180.07	6.74	69.73	12.94 E-06
180.74	6.75	69.86	12.94 E-06
184.94	6.85	70.67	12.94 E-06
166.31	6.39	67.02	12.94 E-06
159.75	6.22	65.68	12.94 E-06
180.55	6.75	69.83	12.94 E-06
173.58	6.57	68.46	12.94 E-06
197.61	7.17	73.05	12.94 E-06
182.44	6.80	70.19	12.94 E-06
164.35	6.34	66.62	12.94 E-06

Table 5.2: Real values of Bo, Ga and Mo for a water – glycerol mixture (transition regime) of 73.05% in weight of gycerol at 24.3º C (26.32 cP).

Finally, in table 5.3 the comparison with the values by Cano-Lozano et al. [4] is displayed.

	STABLE REGIME				TRANSITION REGIME			
	Volume (mm^3)	Bo	Ga	Mo	Volume (mm^3)	Bo	Ga	Mo
Average	14.83	4.24	52.67	9.87E-06	176.65	8.47	88.49	9.90E-06
Target	16.18	5.00	59.61	9.90E-06	179.71	8.5	88.74	9.90E-06
Relative error	8.34%	15.2%	11.6%	0.30%	1.81%	0.36%	0.29%	0.00%

Table 5.3: Comparison between the obtained values and the target values **[4]**.

A significant difference in the dimensionless numbers can be appreciated for the first case. However, the chosen nozzle diameter was larger than that derived from *Fritz* volume hypothesis for manufacturing reasons; hence it can be assumed that the bubbles are in the wanted regime. In the second case, the obtained values are close enough to target.

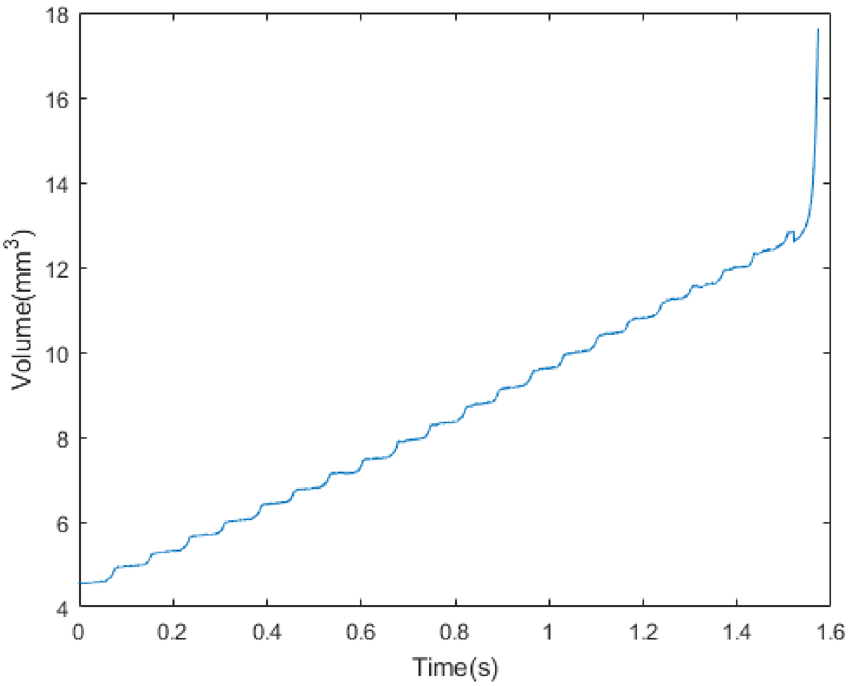

Figure 5.1: Time evolution of the volume of a forming bubble. The constantly increasing part of the graph corresponds to expansion stage while the rapidly increasing end corresponds to collapse stage.

Concerning the volume, although smaller, an appreciable discrepancy exists, and the difference in the nozzle diameter may be a reason for this. Nonetheless, in figure 5.1 it can be observed that the time evolution of the volume increases more or less constantly within the expansion stage of the formation of a bubble and it only accelerates close to collapse. Thus, the air flow can be considered constant during most of the process.

Eliminating the collapse stage, and performing a polynomial fit, the air flow obtained from the slope of this fit results 5.50 mm^3/s (see figure 5.2).

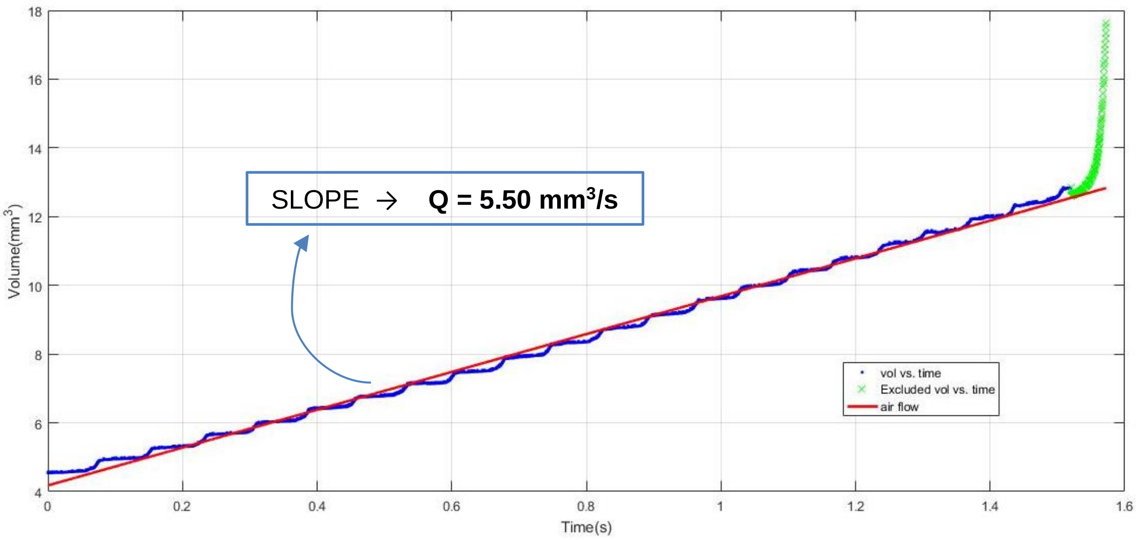

Figure 5.2: Polynomial fit of the expansion stage of the bubble shows a constant slope of 5.50 mm^3/s.

For these flow conditions and considering the diameter of the orifice (1 mm), the critical flow rate can be calculated as follows:

$$Q_c = \pi \sqrt[6]{\frac{16}{3g^2}\left(\frac{\sigma \cdot d}{2\rho}\right)^5} = \begin{cases} stable\ regime \rightarrow\ Q_c = 447.5\ mm^3/s \\ transition\ regime \rightarrow Q_c = 992.7\ mm^3/s \end{cases}$$

The fact that the air flow is almost constant and far below the critical value, reaffirms the valid usage of *Fritz* volume hypothesis.

5.2. Centroid trajectory

The main issue in this work is to analyse the changes in the trajectory of the bubble when the influence of the wall is introduced.

5.2.1. Stable regime (silicon oil)

Case	Liquid	Mo	Bo	Ga	St	Path	Wake	Regime
22	T11	9.9×10^{-6}	5.0	59.61		rectilinear	axisymmetric	rectilinear
23	T11	9.9×10^{-6}	6.0	68.34		rectilinear	axisymmetric	rectilinear

Table 5.4: Characteristic properties of the stable flow conditions considered in the study by Cano-Lozano et al. **[4]**.

Firstly, the bubbles in the stable regime (corresponding to bubbles 22 and 23 in table 5.4) were tested. Without the wall, they performed a regular rectilinear path. As shown in figures 5.4, 5.6 and 5.8, the behaviour was significantly different depending on the position of the vertical surface. For that reason, three values of S (s/D) were analysed.

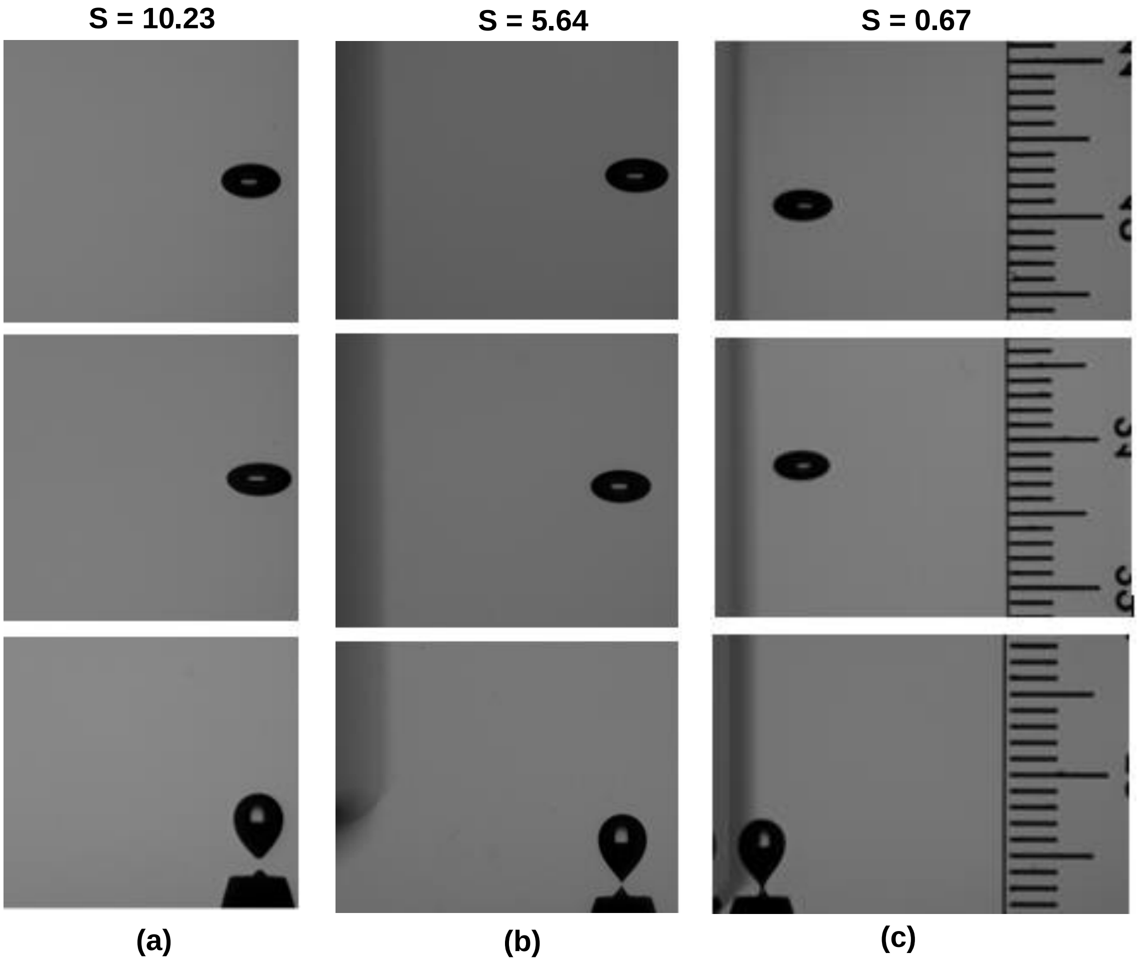

Figure 5.3: Sequential snapshots of the experiments at different heights from the injector (lowest, medium, highest) for (a) S = 10.23 (wall is so far it does not appear in the picture); (b) S = 5.64 and (c) S = 0.67.

In the graphs, the dimensionless coordinates of the bubble centroid were represented, were X stands for coordinate x divided over the bubble equivalent diameter and Y stands for coordinate y divided over the bubble equivalent diameter.

It is noted that the origin of the trajectories is set to be the centroid of the bubble in the instant it detaches from the nozzle and the wall is represented by a cyan line at the left hand side of each graph.

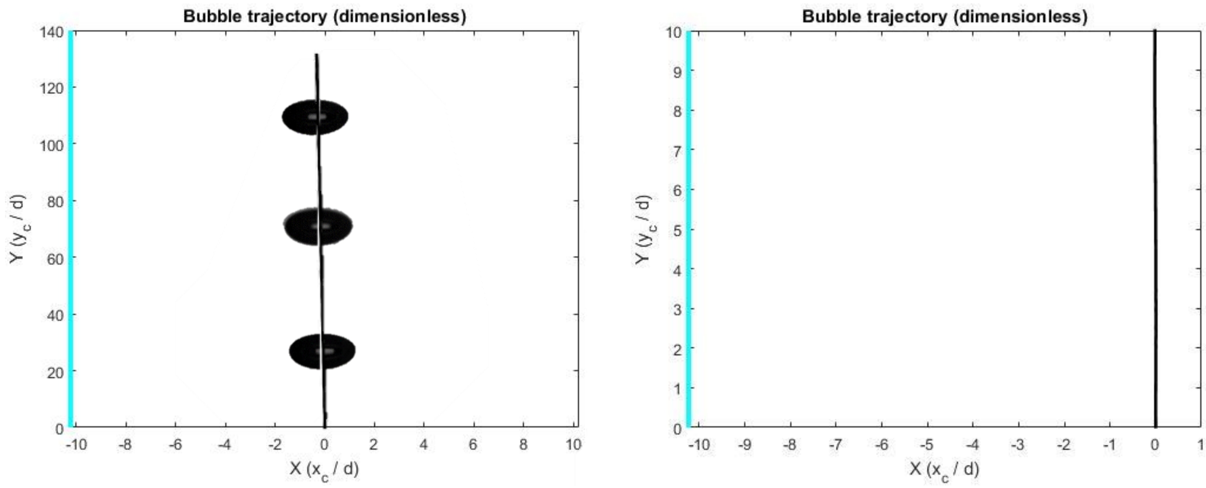

(a) **(b)**

Figure 5.4: Path of a bubble in the stable regime for a value of S of 10.23. Figure (a) shows the full path while (b) shows only the initial behaviour after detachment (until y = 10D).

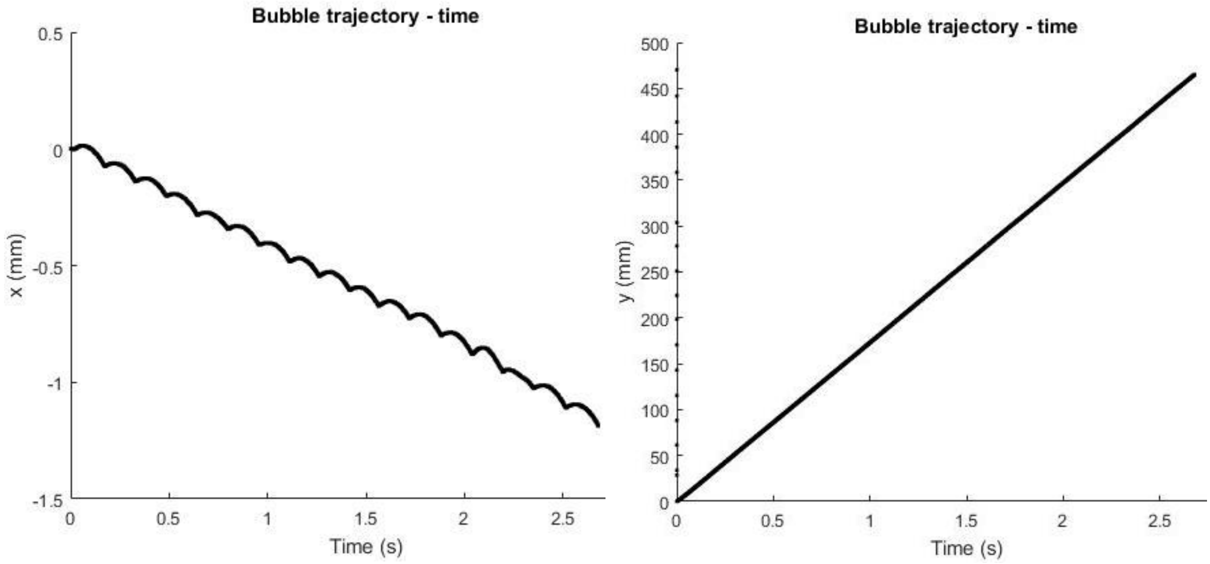

(a) **(b)**

Figure 5.5: Time evolution of the trajectory of a bubble in the stable regime for a value of S of 10.23. Figure (a) shows the horizontal displacement while (b) shows the vertical displacement.

For the largest value of S (10.23) only slight influence of the wall was observed (around 1 mm of horizontal displacement in 500 mm of vertical displacement); hence it can be assumed that the distance to the surface was too large.

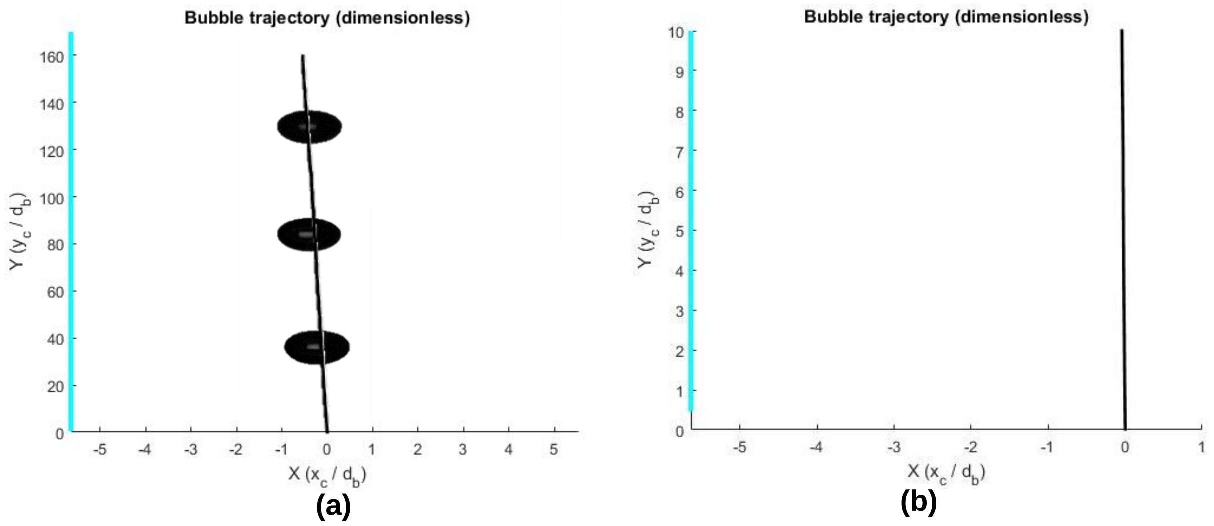

Figure 5.6. Path of a bubble in the stable regime for a value of S of 5.64. Figure (a) shows the full path while (b) shows only the initial behaviour after detachment (until y = 10D).

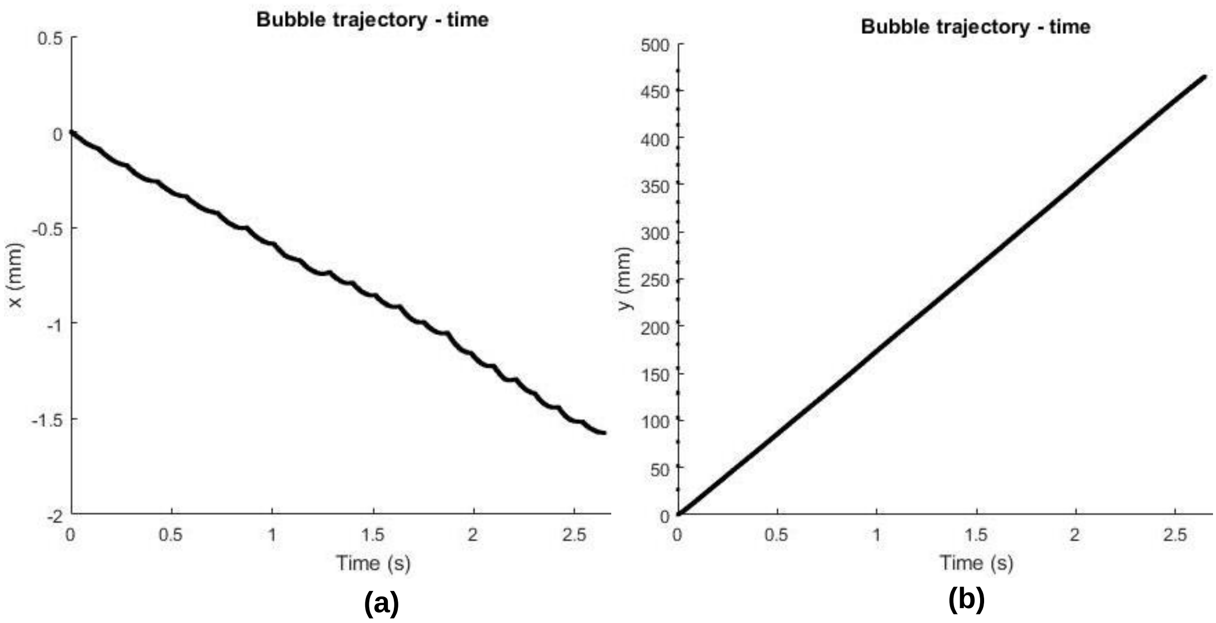

Figure 5.7: Time evolution of the trajectory of a bubble in the stable regime for a value of S of 5.64. Figure (a) shows the horizontal displacement while (b) shows the vertical displacement.

On the other hand, a smaller value of S (5.64) showed more influence of the wall in the trajectory of the bubbles. They experimented a slow migration towards the wall (around 1.5 mm) throughout the entire height of the tank.

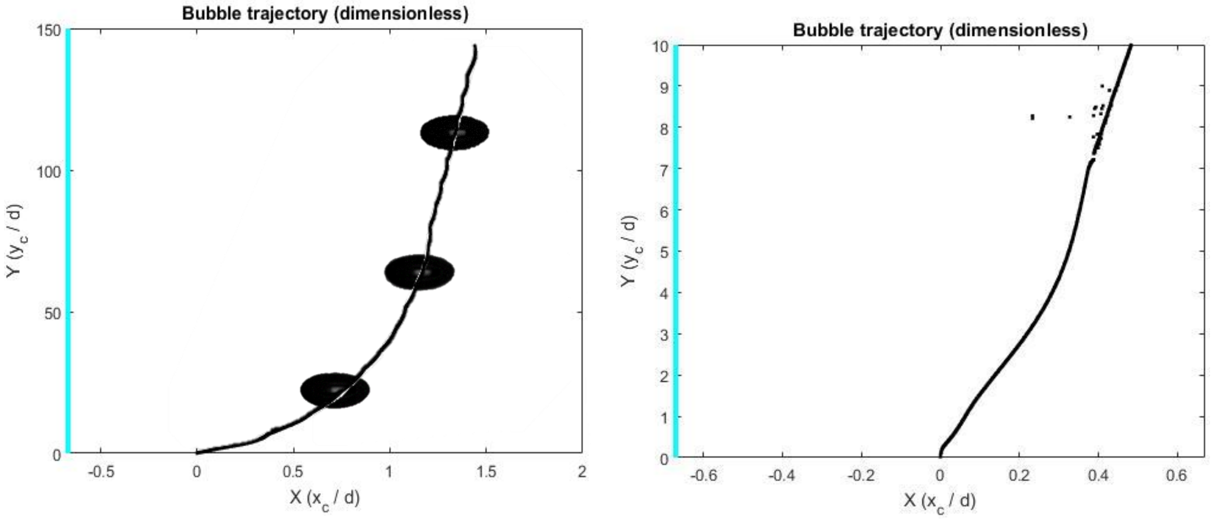

(a) (b)

Figure 5.8: Path of a bubble in the stable regime for a value of S of 0.67. Figure (a) shows the full path while (b) shows only the initial behaviour after detachment (until y = 10D).

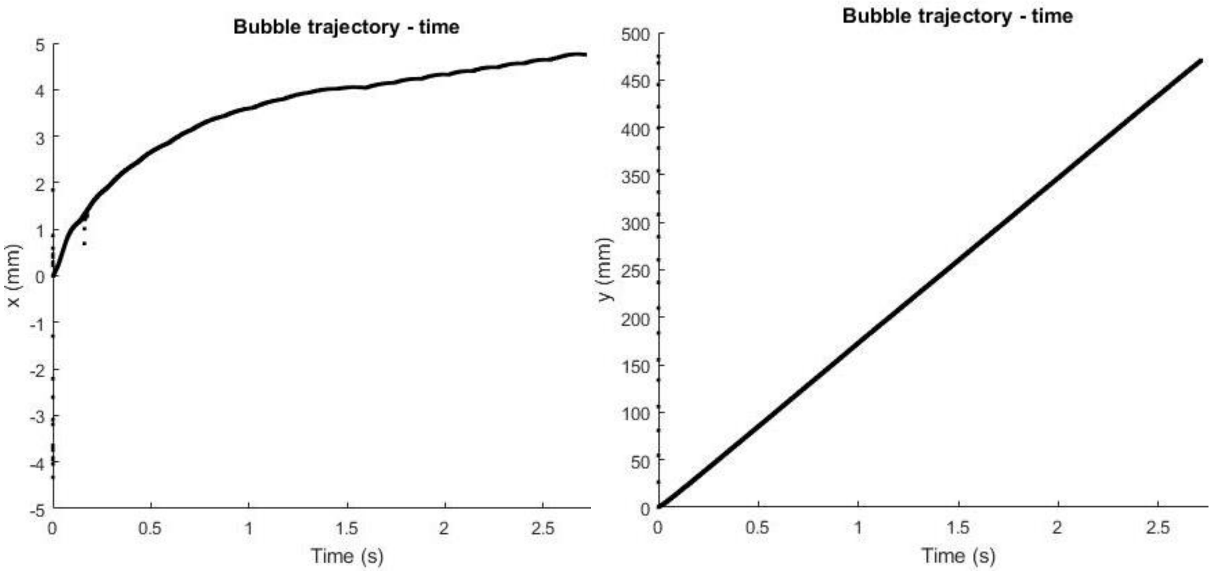

(a) (b)

Figure 5.9: Time evolution of the trajectory of a bubble in the stable regime for a value of S of 0.67. Figure (a) shows the horizontal displacement while (b) shows the vertical displacement.

Finally, a completely distinct behaviour was observed for the smallest value of S (0.670). Note that S is smaller than 1 (meaning that the bubbles were larger in diameter than was their distance to the wall), but also larger than 0.5 (assuring the bubbles will not touch or bounce on the wall). In this case, the bubbles seemed to migrate away from the wall fast after detachment to continue this migration but at a slower pace along the rest of the trajectory (up to 5 mm).

5.2.2. Transition regime (water – glycerol mixture)

Case	Liquid	Mo	Bo	Ga	St	Path	Wake	Regime
24	T11	9.9×10^{-6}	7.0	76.72	0.120	planar zigzag	2CRV 2R	zigzagging
25	T11	9.9×10^{-6}	8.5	88.74	0.132	planar zigzag	2CRV 2R	zigzagging
26	T11	9.9×10^{-6}	10.0	100.25	$0.136 \rightarrow 0.174$	planar zigzag →	spiral	spiraling

Table 5.5: Characteristic properties of the transitional flow conditions considered in the study by Cano-Lozano et al. **[4]**.

Additionally, the same routine was developed for the bubbles in the transition regime. In these cases, the behaviour without wall was characterized in detail because the larger size of the bubbles caused oscillations. Therefore, the rising bubble was recorded without wall and with the wall for two values of S: 4.18 and 2.36.

no wall **S = 4.18** **S = 2.36**

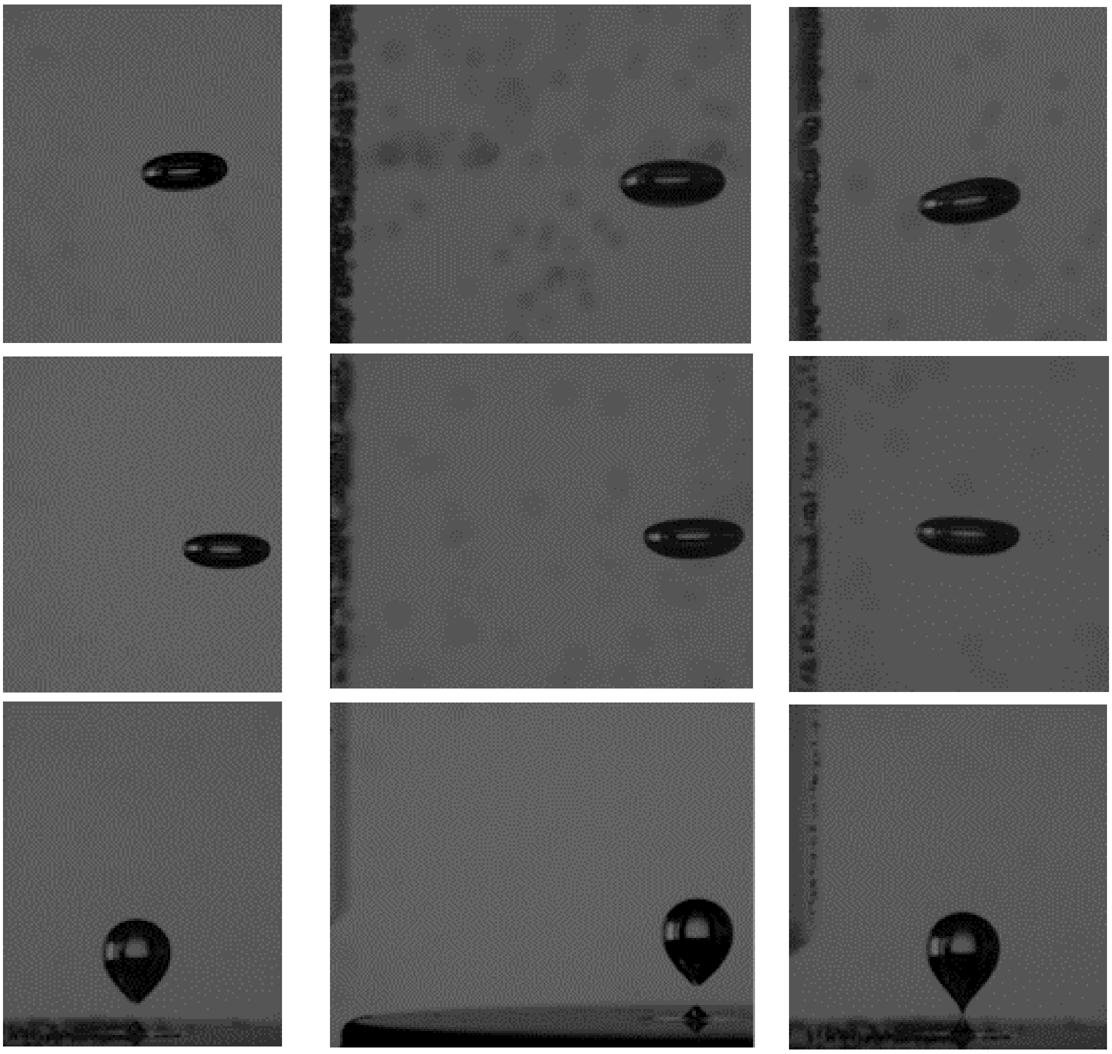

(a) **(b)** **(c)**

Figure 5.10: Sequential snapshots of the experiments at different heights from the injector (lowest, medium, highest) for (a) without the wall; (b) S = 4.18 and (c) S = 2.36.

The behaviour for the first value of S (4.18) (figure 5.11) showed only small differences to that without the wall, thus it is so far from the bubbles that its influence is negligible. Note that the wall is represented by a cyan line at the left hand side of the graph, the unaltered behaviour is shown in red and the trajectory affected by the wall is marked by black dots.

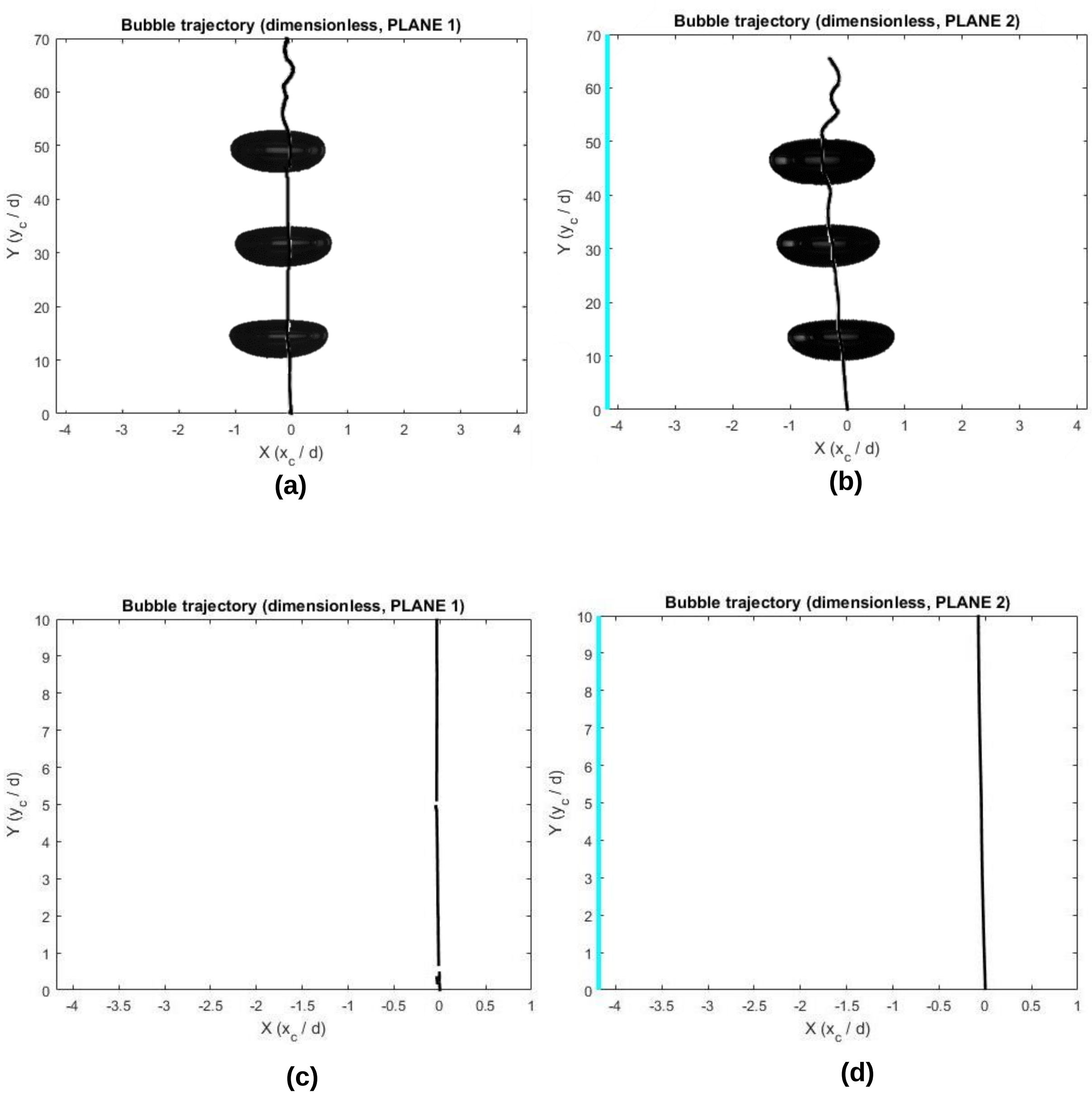

Figure 5.11: Path of a bubble in the transitional regime for a value of S of 4.18. Figures (a) and (b) show the full path while (c) and (d) show only the initial behaviour after detachment (until y = 10D). On the left hand side the plane parallel to the wall is displayed (plane 1) while the perpendicular plane is plane 2 (right hand side).

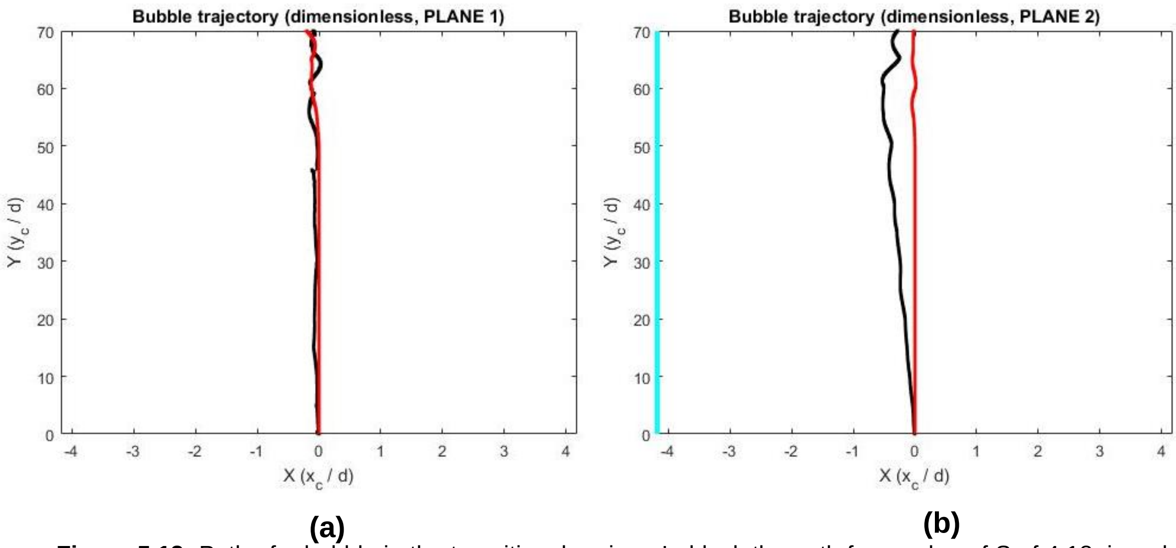

Figure 5.12: Path of a bubble in the transitional regime. In black the path for a value of S of 4.18; in red the path without wall. On the left hand side the plane parallel to the wall is displayed (plane 1) while the perpendicular plane is plane 2 (right hand side).

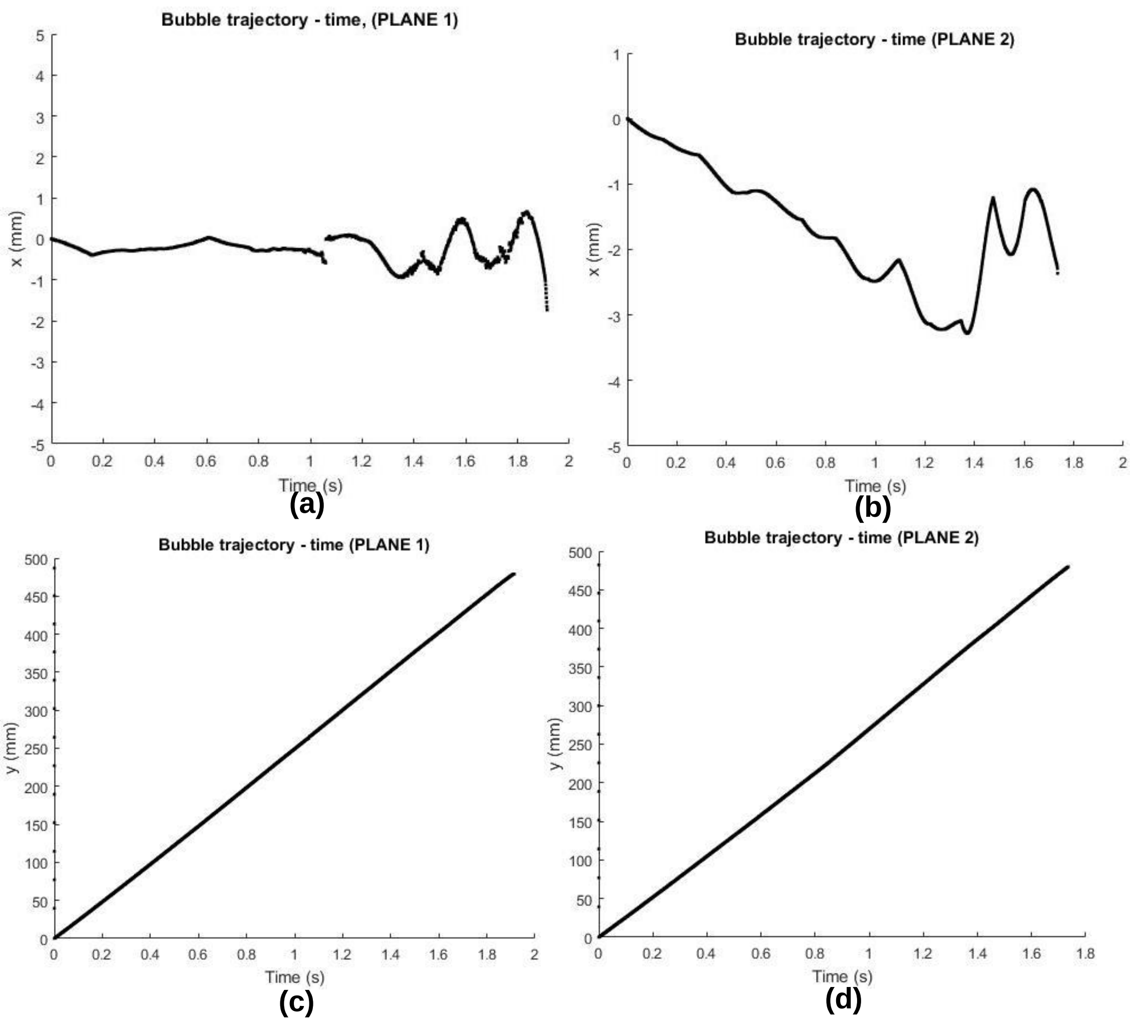

Figure 5.13: Time evolution of the trajectory of a bubble in the transitional regime for a value of S of 4.18. Figures (a) and (b) show the horizontal displacement while (c) and (d) show the vertical displacement. On the left hand side the plane parallel to the wall is displayed (plane 1) while the perpendicular plane is plane 2 (right hand side).

On the other hand, for S = 2.36, the distance was closer and the influence was more pronounced. Figure 5.14 shows how the bubbles tend to migrate away from the wall, similarly to the behaviour in the rectilinear regime for S = 0.67. The oscillations amplitude seem to increase too; especially, perpendicularly to the wall (plane 2).

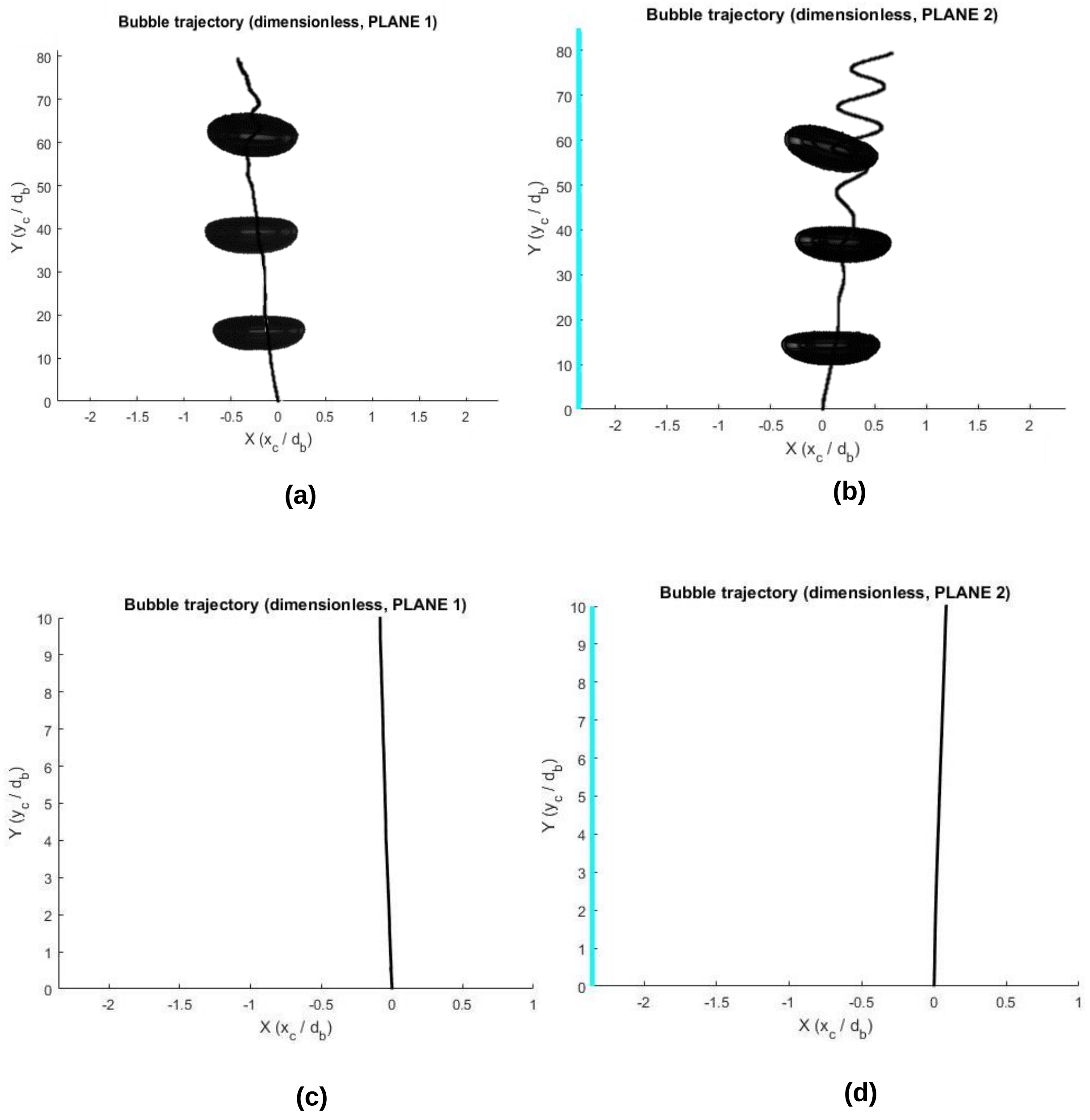

Figure 5.14: Path of a bubble in the transitional regime for a value of S of 2.36. Figures (a) and (b) show the full path while (c) and (d) show only the initial behaviour after detachment (until y = 10D). On the left hand side the plane parallel to the wall is displayed (plane 1) while the perpendicular plane is plane 2 (right hand side).

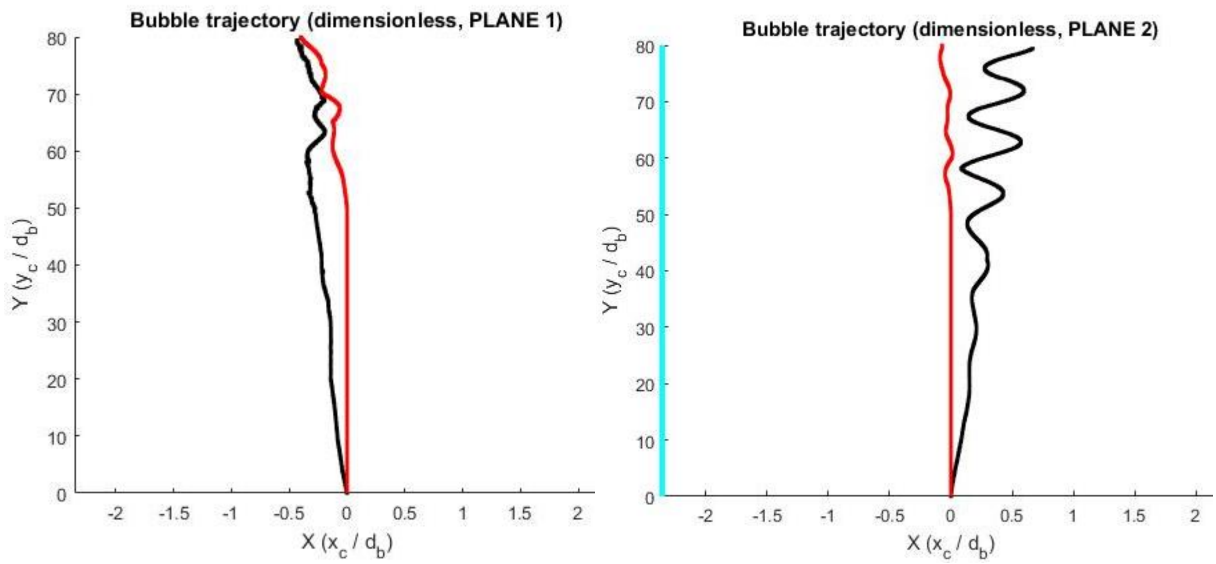

(a) (b)

Figure 5.15: Path of a bubble in the transitional regime. In black the path for a value of S of 2.36; in red the path without wall. On the left hand side the plane parallel to the wall is displayed (plane 1) while the perpendicular plane is plane 2 (right hand side).

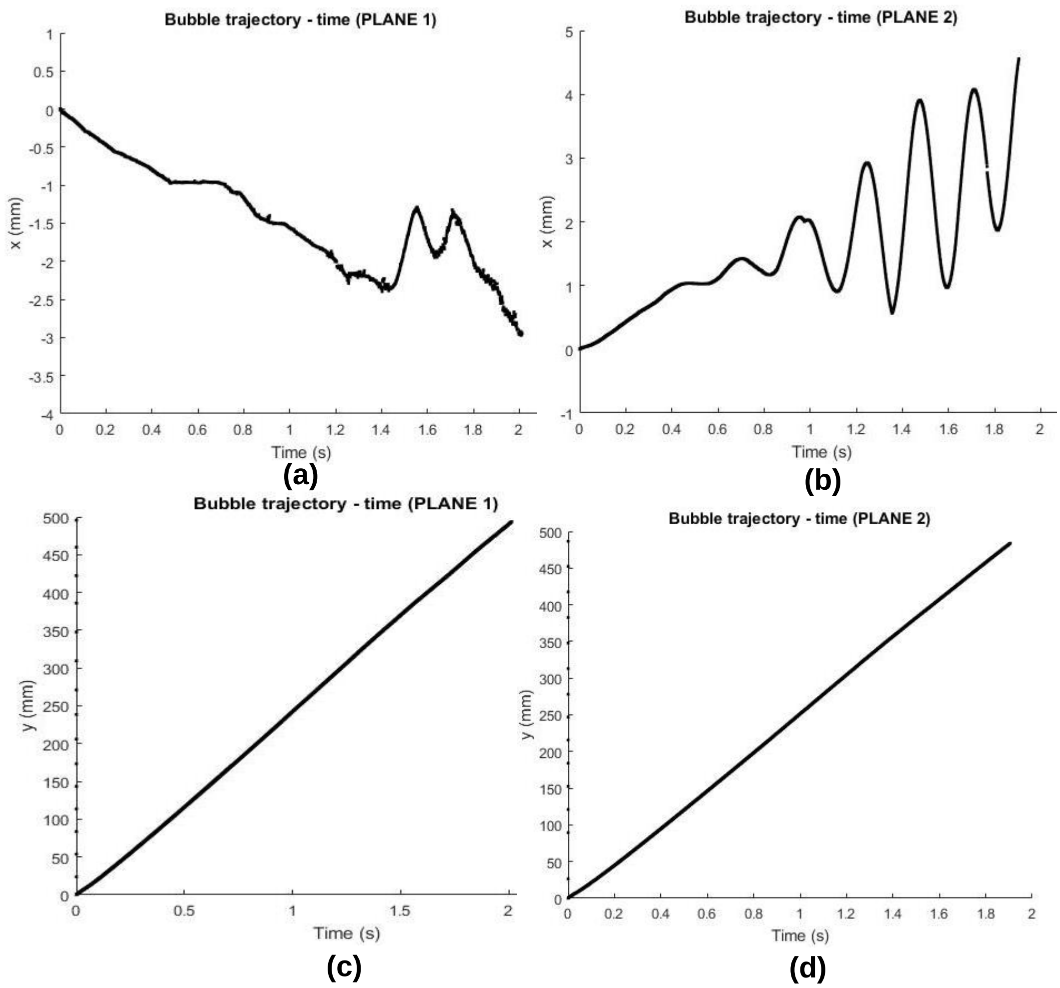

Figure 5.16: Time evolution of the trajectory of a bubble in the transitional regime for a value of S of 2.36. Figures (a) and (b) show the horizontal displacement while (c) and (d) show the vertical displacement. On the left hand side the plane parallel to the wall is displayed (plane 1) while the perpendicular plane is plane 2 (right hand side).

5.3. Velocity

The velocity of the bubble was calculated in order to compare the terminal velocity obtained with that from the bibliography, validating the experiments.

It is marked that the experimental values for the velocity were obtained by performing a centred differentiation of the trajectory over time.

5.3.1. Stable regime (silicon oil)

For the bubbles in the stable regime, horizontal velocity showed in the three cases (for the three different values of S) small amplitude oscillations around zero, meaning the movement towards or away from the wall was small and slow, thus the trajectories were close to rectilinear.

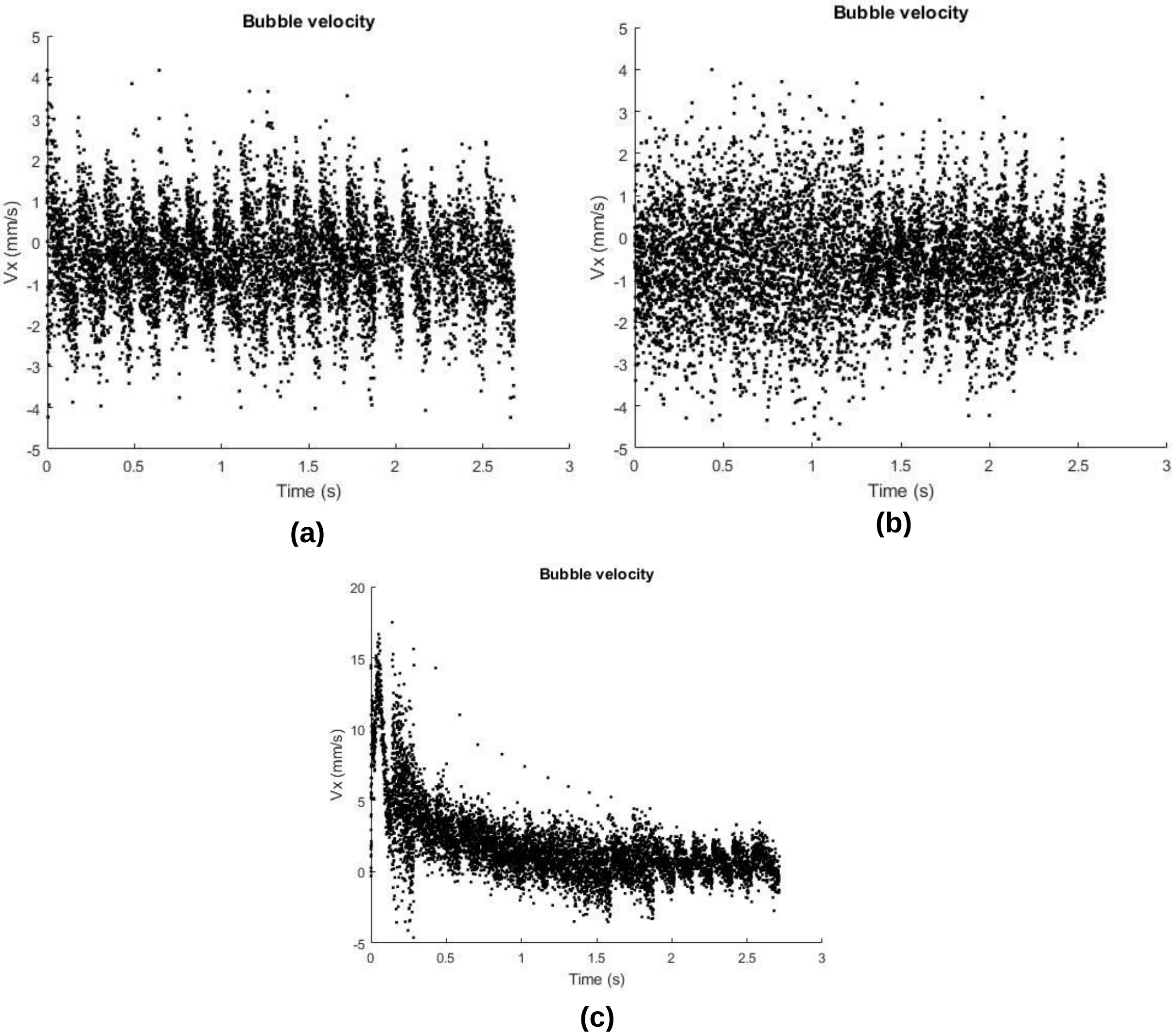

Figure 5.17: Horizontal velocity of bubbles in the stable regime for a value of S of (a) 10.23, (b) 5.64 and (c) 0.67.

The vertical velocity displayed a different behaviour. As expected, the bubble detaches from the nozzle at an increasing speed and decelerates until it reaches a constant rise velocity when lift and viscosity effects compensate each other.

This could be appreciated before in figures 5.5, 5.7 and 5.9, which showed a constant slope in the vertical trajectory that seemed in deed, similar in the three cases.

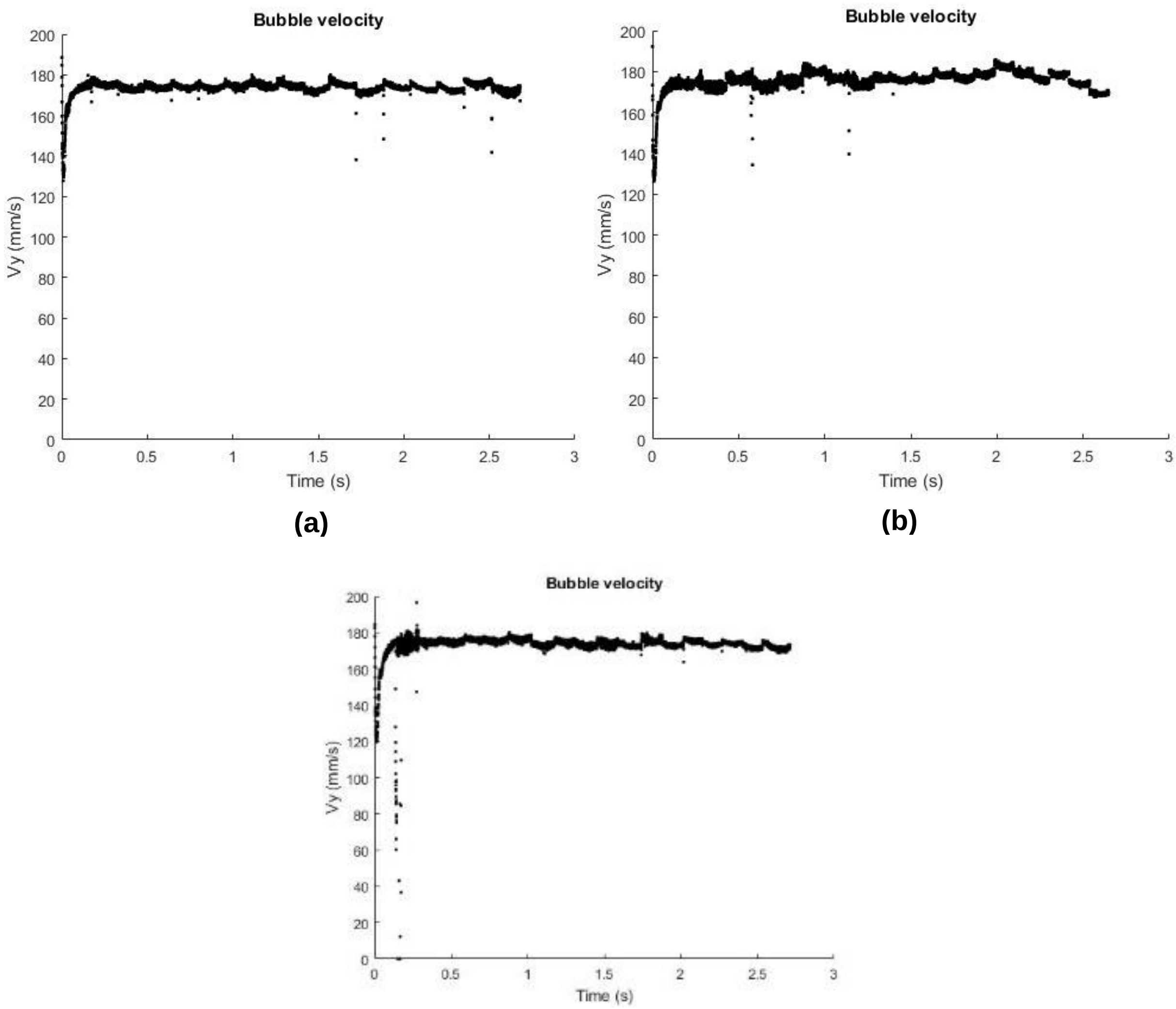

(a) (b) (c)

Figure 5.18: Rising velocity of bubbles in the stable regime for a value of S of (a) 10.23, (b) 5.64 and (c) 0.67.

From figure 5.18 it can be deduced that the terminal velocity for the three cases is the same and its value is around 172 mm/s.

5.3.2. Transition regime (water – glycerol mixture)

Running the same routine for the transition regime, the rising velocity for the largest bubbles is found to be stabilize around 250 mm/s. It shows a constant value for the rectilinear part of the path and tends to slightly decelerate and oscillate when starting to zigzag.

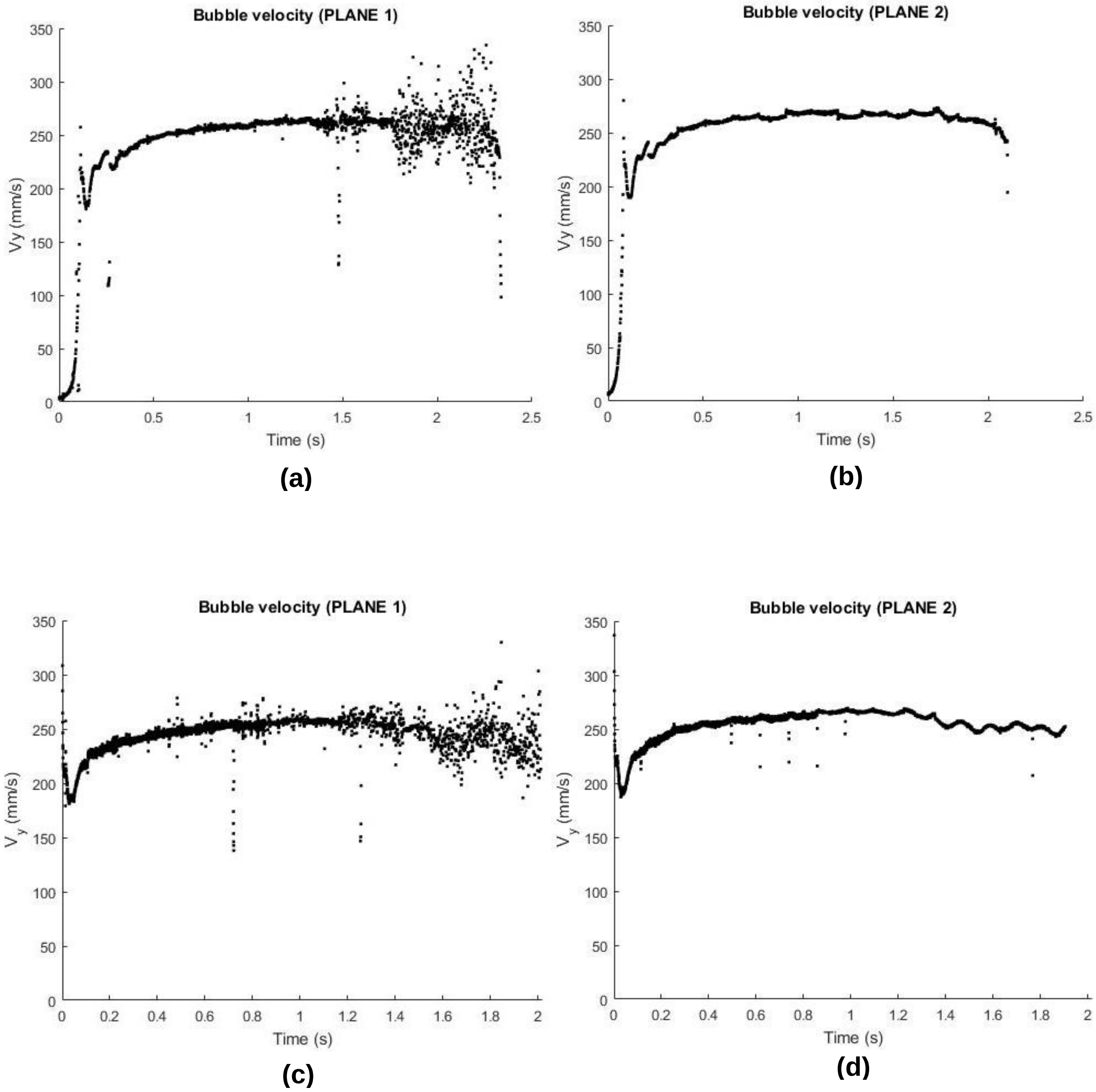

Figure 5.19: Rising velocity of bubbles in the transition regime for a value of S of (a), (b) 4.18 and (c), (d) 2.36. On the left hand side the plane parallel to the wall is displayed (plane 1) while the perpendicular plane is plane 2 (right hand side).

The horizontal velocity kept its around-zero-value until the beginning of the zigzagging path.

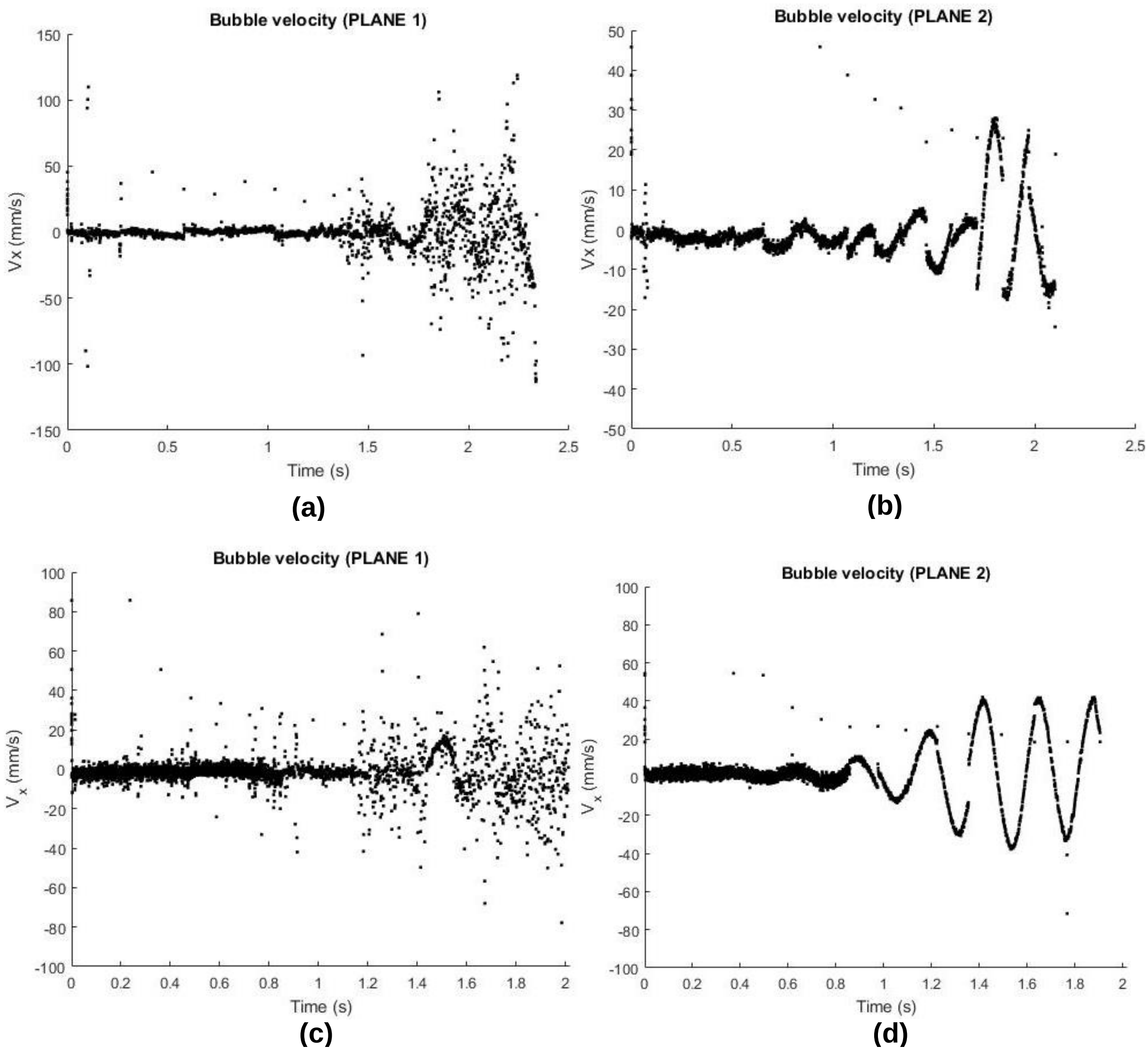

Figure 5.20: Horizontal velocity of bubbles in the transition regime for a value of S of (a), (b) 4.18 and (c), (d) 2.36. On the left hand side the plane parallel to the wall is displayed (plane 1) while the perpendicular plane is plane 2 (right hand side).

5.3.3. Comparison to cases without wall

Figure 5.21 shows a theoretical correlation by Clift et al. [16] which considers Mo, Bo (a.k.a. Eötvos number) and Reynolds number (Re). Defining Re for the equivalent diameter of the bubble and its terminal velocity, the latter can be derived from the graph and compared to the experimental values.

D (mm)	Bo	Mo	Log (Mo)	Re	v_∞ (mm/s)	Error (%)
3.05	4.245	9.87 E-06	-5.006	60	196.72	12.57%
6.82	8.47	9.90E-06	-5.004	87	261.93	2.65%

Table 5.6: Velocity of a freely rising bubble according the correlation by Clift et al. **[16]** and comparison to experimental results.

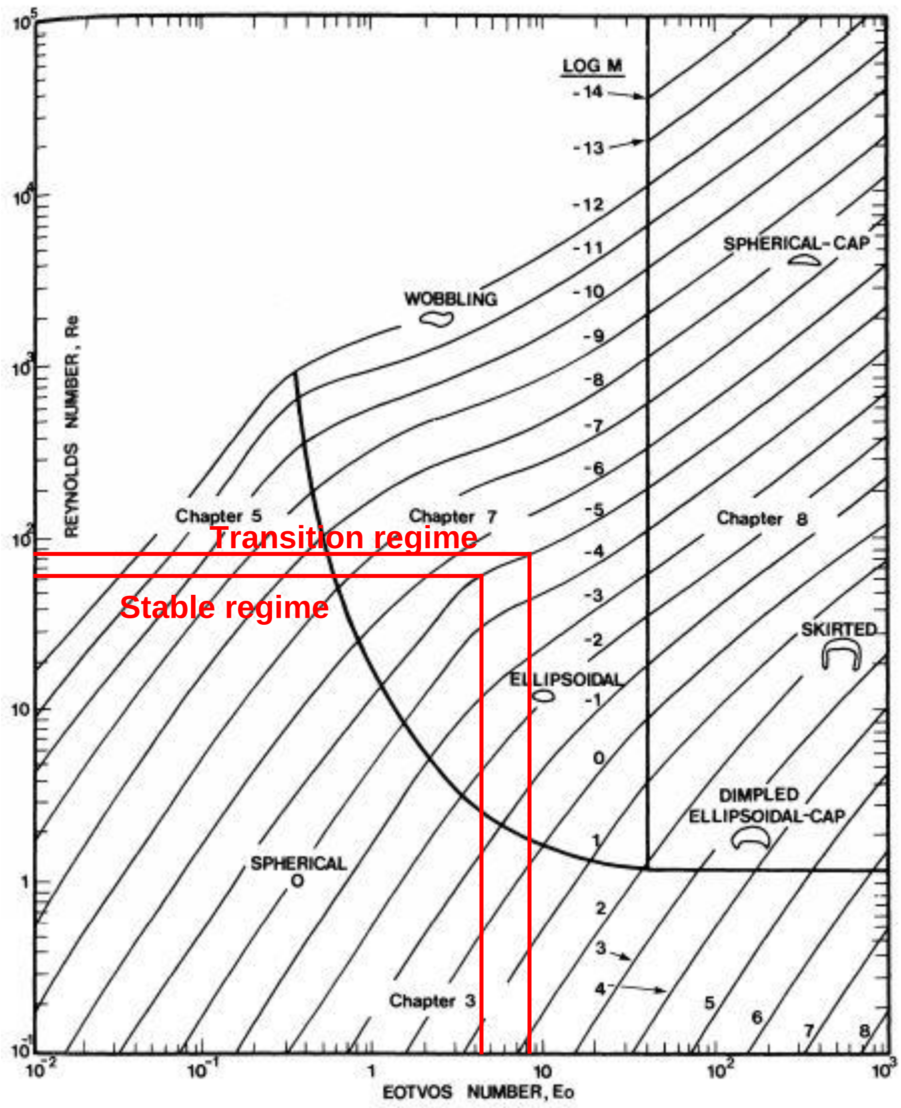

Figure 5.21: Velocity of a freely rising bubble according the correlation by Clift et al. **[16]**

The error found for the rectilinear regime shows that the bubble suffers a slight deceleration when placing the wall. Concerning the transition regime, the rise velocity is found to remain almost unaltered.

6. CONCLUSIONS AND FUTURE WORK

In this work, different cases of bubbles rising close to a vertical wall were experimentally tested, recorded and processed.

The experiments were developed in a 60x15x15 cm glass tank with a moveable wall. The air came from an inlet at the bottom centre of the tank and the bubble formed was allowed to rise freely through its height. The experiments covered two different sizes for the air nozzle (hence, for the bubble equivalent diameter D) and three different distances between the bubble and the wall.

The bubbles were recorded using high speed cameras and every video was post–processed in order to collect the information from the experiments. The analysis consisted on separating the videos into individual frames, calculating the properties of each bubble (namely centroid, area and volume) and aligning those frames to compound a full trajectory. Thanks to this process several findings were achieved:

Firstly, bubbles in the stable regime were tested. The trajectory followed by these bubbles ought to be rectilinear. However, their behaviour changed when the wall was placed in their proximity.

It was observed that the closer the wall was placed, the closer the bubbles migrated towards the wall. Nevertheless, when the distance became too small (< D), the bubbles tended to migrate away from the wall, thus moving in the opposite direction.

Secondly, the same experiments were run with larger bubbles (transition regime). Without the wall, these bubbled showed a firstly rectilinear path that started oscillating by the higher half of the tank.

When placing the wall, the trajectories performed similar changes to those of the stable regime: for large distances between the wall and the bubble, the latter moved towards the wall while it migrated away from it when the distance became very small. However, the critical value of this distance that causes the change of direction resulted larger for the transition regime (e. g. 2.36D) than for the stable regime.

In both regimes, no differences were appreciated in the trajectory in the perpendicular direction (wall plane) and only a slight deceleration in the rising velocity.

To conclude, this work can be extended as a Master's degree Thesis, in which several aspects that this work could not cover can be developed:

In both regimes, different bubble diameters could be tested in order to cover other regions of the Ga – Bo plane. This would help determine the relevance of bubble size in the problem and how the wall affects the transition between regimes.

Furthermore, numerical simulations could be performed in order to compare their results to those obtained from the experiments developed for this work.

Finally, new laboratory equipment was designed in order to avoid misalignments of consecutive recorded windows, which involved excessive image post-processing. This system consists on a linear engine that assures precise and synchronous vertical movement of both cameras. This new set-up is expected to be installed for the coming experimentation.

REFERENCES

[1] R. Bolaños-Jiménez, Dynamics of bubble formation in cylindrical and planar geometries, Jaén: Universidad de Jaén, 2011.

[2] J. M. Gordillo, A. Sevilla, J. Rodríguez-Rodríguez and C. Martínez-Bazán, “Axisymmetric bubble pinch-off at high reynolds numbers,” *Physical Review Letters,* vol. 95, p. 194501, 1 November 2005.

[3] H. N. Oguz and A. Prosperetti, “Dynamics of bubble growth and detachment from a needle,” *Journal of Fluid Mechanics,* vol. 257, no. 1, pp. 111-145, 1993.

[4] J. C. Cano-Lozano, C. Martínez-Bazán, J. Magnaudet and J. Tchoufag, “Paths and wakes of deformable nearly spheroidal rising bubbles close to the transition to path instability,” *Physical Review Fluids,* vol. 1, no. 5, pp. 053604/1-053604/30, 2016.

[5] J. Lee and H. Park, “Wake structures behind an oscillating bubble rising colse to a vertical wall,” *International Journal of Multiphase Flow,* vol. 91, pp. 225-242, 2017.

[6] H. Jeong and H. Park, “Near-wall rising behavioour of a deformable bubble at high reynolds number.,” *Journal of Fluid Mechanics,* vol. 771, pp. 564-594.

[7] A. de Vries, A. Biesheuvel and L. van Wijngaarden, “Notes on the path and wake of a gas bubble rising in pure water,” *International Journal of Multiphase Flow,* vol. 28, no. 11, pp. 1823-1835, November 2002.

[8] Y. Fu and Y. Liu, “Experimental study of bubbly flow using image processing techniques,” *Nuclear Engineering and Design,* vol. 310, pp. 570-579, 15 December 2016.

[9] C. Bongiovanni, A. Dominguez and J. P. Chevaillier, “Understanding images of bubbles,” *European Journal of Physics,* vol. 21, pp. 561-570, 2000.

[10] N. Otsu, “A Threshold Selection Method from Gray-Level Histograms,” *IEEE TRANSACTIONS ON SYSTEMS, MAN, AND CYBERNETICS,* vol. 9, no. 1, January 1979.

[11] J. Cano-Lozano, P. Bohorquez and C. Martínez-Bazán, “Wake instability of a fixed axisymmetric bubble of realistic shape,” *International Journal of Multiphase Flow,* vol. 51, pp. 11-21, 2013.

[12] I. Eames and J. Magnaudet, “The motion of high-Reynolds number bubbles in inhomogeneus flows,” *Annual Review of Fluid Mechanichs,* vol. 32, pp. 659-708, 2000.

[13] Y. Tagawa, S. Takagi and Y. Matsumoto, “Surfactant effect on path instability of a rising bubble,” *Journal of Flid Mechanics,* vol. 738, pp. 124-142, 2014.

[14] R. Zenit and J. Magnaudet, “Path instability of rising spheroidal air bubbles: A shape-controlled process,” *Physics of Fluids,* vol. 20, 2008.

[15] C. S. Miner and N. N. Dalton, Physical Properties of Glycerine and Its Solutions, Reinhold Publishing Corp., 1953.

[16] R. Clift, J. R. Grace and M. E. Weber, Bubbles, Drops and Particles, New York, San Francisco, London: Academic Press, 1978.

APPENDIX A: Codes

A.1. Main code for volume calculation (MATLAB)

```
% MAIN
close all
clear
clc

% Data initialization
num_vid = input('Video number: ','s');
video = ['vid_',num2str(num_vid)];
frames = input('Video frame number: ');
% fps = input('Capture velocity (fps): ');
if frames > 300
    fps = 3000;
else
    fps = 1000;
end
d_tob = seleccion_tobera;
dist = menu('DISTANCE TANK-WALL', 'no wall', '3 cm','5 cm');
    switch dist
        case 1
            dist = 'no wall';
        case 2
            dist = 3;
        case 3
            dist = 5;
    end

% Video discretization
[carp_v,carp_i] = avi2tiff(video, frames, dist, d_tob);

%Image processing
time = zeros(1,frames);
area = zeros(1,frames);
vol = zeros(1,frames);
cent = zeros(frames,2);
xim = 0;
yim = 0;

for i=1:frames
    imagen = [carp_i,num2str(video),'_',num2str(i),'.tif'];
    % Scale mm/píxel
    if i==1
        unidad = menu('Resolution reference (mm)',1,5,10); % unit mm from
image
        im_REGLA = [carp_v,num2str(video),'_REGLA.tif'];
        esc = escala(unidad, im_REGLA);
    end

    [bw,cont,properties,xim,yim] = deteccion_filo(imagen,i,xim,yim);

    % Centroid
    c = properties.Centroid;
    c(:,1)=c(:,1)+xim(1);
    c(:,2)=c(:,2)+yim(1);
    cent(i,:) = c;
    hold on
    plot(c(:,1),c(:,2), 'y*');
```

```
    pause(0.7);

    % Section
    area(i) = properties.Area;
    area = area.*(esc^2);

    %Volume
    vol(i) = calc_vol(cont, esc);

    if i<frames
        time(i+1)=time(i)+1/fps;
    end
end
clc
close all

%Centroid plot
figure(2), title('Trayectoria burbuja');
plot(cent(:,1),-cent(:,2),'o');
hold off
axis([min(cent(:,1))-3,max(cent(:,1))+3,-max(cent(:,2)),-min(cent(:,2))]);

%Fluid
[rho,mu,sigma] = seleccion_fluido;
clc

%Dimensionless numbers
d = (((0.75.*vol/pi).^(1/3))*1e-3)*2;
g = 9.81; %m/s^2

Bo = rho*g*(d.^2)/sigma;
Ga = (sqrt(g*d)*rho.*d)/mu;
Mo = (Bo.^3)./(Ga.^4);

% vol_m = sum(vol)/length(vol);Bo_m = sum(Bo)/length(Bo); Ga_m =
sum(Ga)/length(Ga); Mo_m = sum(Mo)/length(Mo);
% fprintf('Valores medios del volumen y los adimensionales:\n v = %f;  Bo =
%f;  Ga = %f;  Mo = %d; \n \n' ,vol_m,Bo_m,Ga_m,Mo_m);

% fprintf('Valores iniciales del volumen y los adimensionales:\n v = %f;
Bo = %f;  Ga = %f;  Mo = %d; \n',vol(1),Bo(1),Ga(1),Mo(1));

v_Fritz = pi*d_tob*sigma/rho/g*1e6;
err = abs(vol(1)-v_Fritz)/v_Fritz*100;
% fprintf('Error relativo entre hipótesis de Fritz y volumen real =
%f%%;\n',err);

clc
nom_mat = [num2str(video),'_centroide.mat'];
matriz_centroide=[cent(:,1)';-cent(:,2)';time];
save([carp_v,num2str(nom_mat)],'matriz_centroide');

load('calib.mat');
m = find(calib==0,1);
calib(m)=esc;
save('calib.mat','calib');

nom_mat = [num2str(video),'_vol.mat'];
matriz_vol=[Bo(1), Ga(1), Mo(1); vol(1),v_Fritz,err];
```

```
save([carp_v,num2str(nom_mat)],'matriz_vol');

disp('Data was correctly saved');
close all
```

A.1.1. Function for separating frames

```
% Save video images

function [carp_v,carp_i] = avi2tiff(video, frames, dist)
% carp_v = 'C:\Users\CeciliaEC\Desktop\UJA\TFG + Prácticas\MATLAB\Vídeos\';
carp_v = ['E:\Cámara\ACEITE\PARED\',num2str(dist),'\',num2str(video),'\'];
% carp_i = ['C:\Users\CeciliaEC\Desktop\UJA\TFG +
Prácticas\MATLAB\avi2tiff_images\',num2str(video),'\'];
carp_i = ['E:\Cámara\imag_analisis\',num2str(dist),'\',num2str(video),'\'];
lect = input(' Save images? Y/N: ','s');
if lect=='Y'
    tic
    obj = VideoReader([carp_v,video,'.avi']);
        for k = 1:frames
            im = readFrame(obj);
            nom_img = [carp_i,num2str(video),'_',num2str(k),'.tif'];
            imwrite(im, nom_img);
        end
    toc
end
```

A.1.2. Function for image imbinarization

```
function [BW,maskedImage] = img_binario_modif(X)
%segmentImage Segment image using auto-generated code from imageSegmenter
App
%  [BW,MASKEDIMAGE] = segmentImage(X) segments image X using auto-generated
%  code from the imageSegmenter App. The final segmentation is returned in
%  BW, and a masked image is returned in MASKEDIMAGE.

% Auto-generated by imageSegmenter app on 03-Apr-2019
%----------------------------------------------------



% Threshold image - manual threshold
BW = X > 52;

% Invert mask
BW = imcomplement(BW);

% Fill holes
BW = imfill(BW, 'holes');

% Create masked image.
maskedImage = X;
maskedImage(~BW) = 0;
```

A.1.3. Function for edge detection

```
function [bw,cont,properties,xim,yim] =
deteccion_filo(imagen,frame,xim,yim,dist)
%     close all
    clc
```

```
    X=imread(imagen);

    %Region of interest
    if frame == 1
        figure(1), imshow(X),title('Select bubble movement area');
        [xim,yim] = ginput(2); %Matrix 2x2
        xim = round(xim); % x coordinates of both picked corners
        yim = round(yim); % y coordinates of both picked corners
    end
    imag = X(yim(1):yim(2),xim(1):xim(2));
    boxul(1) = xim(1)-1;  boxul(2) = yim(1)-1;
    if dist~=6
        bw = img_binario(imag);
    else
        bw = img_binario_modif(imag);
    end
    label=logical(bw);

    properties=regionprops(label,'Solidity','Area','centroid');
    density=[properties.Solidity];
    area=[properties.Area];

    high_dense_area=density>0.5;
    max_area=max(area(high_dense_area));
    bubble_label=find(area==max_area);
    bubble=ismember(label,bubble_label);

    se=strel('square',1);
    bubble=imdilate(bubble,se);

    figure(1)
    [cont,~]=bwboundaries(bubble,'noholes');
    imshow(X,[])
    hold on
    for i=1:length(cont)
        plot(cont{i}(:,2)+boxul(1),cont{i}(:,1)+boxul(2),'y','linewidth',1)
    end
    title('Bubble edge')
%     pause(0.8);
%     hold off
end
```

A.1.4. Function for area and centroid calculation

```
function properties = filterRegions(bw)
%filterRegions  Filter BW image using auto-generated code from
imageRegionAnalyzer app.
%  [BW_OUT,PROPERTIES] = filterRegions(BW_IN) filters binary image BW_IN
%  using auto-generated code from the imageRegionAnalyzer App. BW_OUT has
%  had all of the options and filtering selections that were specified in
%  imageRegionAnalyzer applied to it. The PROPERTIES structure contains the
%  attributes of BW_out that were visible in the App.

% Auto-generated by imageRegionAnalyzer app on 26-Jan-2019
%---------------------------------------------------------

BW_out = bw;
```

```
% Get properties.
properties = regionprops(BW_out, {'Area', 'EquivDiameter',
'MajorAxisLength', 'MinorAxisLength', 'Perimeter'});
```

A.1.5. Function for scale calculation

```
% Obtention of vertical scale
function esc = escala(unidad, im_regla)
X=imread(im_regla);
figure(1), imshow(X), title('Select scale area');
[fil,col] = ginput(2);
fil = round(fil,0);
col = round(col,0);
Y = X(col(1):col(2),fil(1):fil(2));
figure(1), imshow(Y), title('Select unit');
% figure(1), imshow(X), title('Select unit');
[~,a] = ginput(2);
a = round(a);
close all
d_pix = a(2)-a(1);
esc = unidad/d_pix;
end
```

A.1.6. Function for volume calculation

```
%Bubble volume with trapezoidal sum (mm^3)
function vol = calc_vol(cont, esc)

z_max = min(cont{1}(:,1));
% z_min = max(cont{1}(:,1));
x_min = min(cont{1}(:,2));
x_max = max(cont{1}(:,2));
x_centroid = round((x_max+x_min)/2);

cont_izq = 0;
cont_dcha = 0;
izq_x = [];
izq_z = [];
dcha_x = [];
dcha_z = [];

for k=1:length(cont{1}(:,1))
    if (cont{1}(k,2)) <= x_centroid
        cont_izq = cont_izq+1;
        izq_x(cont_izq) = cont{1}(k,2);
        izq_z(cont_izq) = cont{1}(k,1);
    else
        cont_dcha = cont_dcha+1;
        dcha_x(cont_dcha) = cont{1}(k,2);
        dcha_z(cont_dcha) = cont{1}(k,1);
    end
end

borde_i = [sortrows(izq_x);sortrows(izq_z)];
borde_d = [sortrows(dcha_x);sortrows(dcha_z)];

borde_i(1,:) = abs(borde_i(1,:)-x_centroid)*esc;
borde_d(1,:) = abs(borde_d(1,:)-x_centroid)*esc;
borde_i(2,:) = abs(borde_i(2,:)-z_max)*esc;
borde_d(2,:) = abs(borde_d(2,:)-z_max)*esc;

vol_d = abs(pi*trapz(borde_i(2,:),borde_i(1,:).^2));
```

```
vol_i = abs(pi*trapz(borde_d(2,:),borde_d(1,:).^2));
vol = 0.5*(vol_d+vol_i);
end
```

A.1.7. Function for fluid selection

```
function [rho,mu,sigma,x] = seleccion_fluido
    fl = menu('SELECTION OF FLUID', 'Silicon oil (T11)', 'Glycerol - Water 
mixture');
    switch fl
        case 1
            rho = 0.935*1000; % kg/m^3
            mu = 0.00935; % Pa/s
            sigma = 20.1e-3; % N/m
            x = 100; %
        case 2
            [x,rho,sigma,mu]=glyc_water_prop;
    end
end
```

A.1.8. Function for inlet selection

```
%INLET DATA
function d_tob = seleccion_tobera
    tob = menu('INLET SELECTION', 'small nozzle', 'small orifice', 'medium 
orifice', 'large orifice');
    switch tob
        case 1
            d_tob = 2.35;
        case 2
            d_tob = 7.40;
        case 3
            d_tob = 10.00;
        case 4
            d_tob = 12.60;
    end
end
```

A.2. Main code for trajectory and velocity plot (MATLAB)

```
clear
close all

load('data_dist.mat');
load('lim_fotogramas_dist_cm.mat');
lim=-lim;
mat = data_dist;
esc = 0.0256; %mm/pix
d_t_o = 2813.0555;
d_t_p = (dist+1)/esc;
d_p_o = d_t_o-d_t_p;

[~,fr_max,vid] = size(mat);
fr = zeros(1,vid);
pos = zeros(1,vid);
t_last = zeros(1,vid);
vel = zeros(2,fr_max,vid);

for i=1:vid
    if mat(1,1,i)~=0
```

```
        fr(i)= find(mat(1,:,i)~=0,1,'last');
        llenos=find(fr~=0);
        pos(i)=find(mat(2,:,i)<lim(i),1,'last');
        for j=1:fr(i)
            if j>pos(i)
                mat(:,j,i)=0;
            end
        end
        prev=llenos(find(llenos<i,1,'last'));
        if i~=1
            dif_y=mat(2,pos(prev),prev)-mat(2,1,i);
            dif_x=mat(1,1,i)-mat(1,pos(prev),prev);
            mat(2,:,i)=mat(2,:,i)+dif_y;
            mat(1,:,i)=mat(1,:,i)-dif_x;
        end
    end
end
dif_inic=d_p_o-data_dist(1,1,1);
mat(1,:,:)=(mat(1,:,:)+dif_inic)/d_p_o;
long=min(min(mat(2,:,:)));
mat(2,:,:)=(mat(2,:,:)-long)/d_p_o;
for i=1:vid
    for k=1:fr(i)
        if pos(i)<k
            mat(:,k,i)=0;
        end
        if mat(1,k,i)~=0
            hold on
            plot(mat(1,k,i),mat(2,k,i),'.k');
        end
    end
end
axis([0,1.05,0,8]);
title('Bubble trajectory (dimensionless)');
xlabel('Horizontal displacement (x centroid / distance to wall)');
ylabel('Vertical displacement (y centroid / distance to wall)');

%velocidad
for i=1:vid
    if pos(i)~=0
        if i~=1
            prev=llenos(find(llenos<i,1,'last'));
            mat(3,:,i)=mat(3,:,i)+t_last(prev);
            for k=1:fr_max
                if pos(i)<k
                    mat(3,k,i)=0;
                end
            end
        end
        t_last(i)=mat(3,pos(i),i);
        [grad,~,~]=gradient(mat);
        vel(1,:,i)=grad(1,:,i)./grad(3,:,i);
        vel(2,:,i)=grad(2,:,i)./grad(3,:,i);
        hold on
        figure(2)
        plot(mat(3,:,i),vel(1,:,i),'.k');
        figure(3)
        plot(mat(3,:,i),vel(2,:,i),'.k');
    end
end
figure(2)
```

```
title('Bubble velocity');
xlabel('Time (s)');
ylabel('Horizontal velocity');
figure(3)
title('Bubble velocity');
xlabel('Time (s)');
ylabel('Vertical velocity');
```

A.2.1. Function for creating 3D matrix of image data

```
% load data matrix
video = x;
carp_v = ['E:\Cámara\ACEITE\PARED\6\vid_',num2str(video),'\'];
load([carp_v,'vid_',num2str(video),'_centroide.mat']);
c_x= matriz_centroide;


% 3D matrix
load('data_x.mat');
data_x(:,:,:) = zeros(3,fr_max,vid_max);
for i=1:length(c_vid)
    for j=1:3
        data_x(j,i,vid)=c_vid(j,i);
    end
end
save('data_x.mat','data_x');
```

A.3. Function for glycerol-water mixture calculation (MATLAB)

```
function [x,rho,sigma,mu]=glyc_water_prop
    clear
    clc

    burb = input('Bubble(S/M/L): ','s');
    Mo = 9.9*1e-6;
    g = 9.81;
    t = 22; %°C
    T = t+273.15;
    switch burb
        case 'S'
            Bo = 7;
            Ga = 76.72;
        case 'M'
            Bo = 8.5;
            Ga = 88.74;
        case 'L'
            Bo = 10;
            Ga = 100.25;
    end

    datos;
    [model_rho, ~] = FIT_rho_3D(x_rho, T_rho, rho_tabla);
    [model_mu, ~] = FIT_mu_3D(x_mu, T_mu, mu_tabla);
    [model_sigma, ~] = FIT_sigma_3D(x_s, T_s, sigma_tabla);

    x=0.01;
    sigue=1;

    while sigue
```

```
        rho = model_rho(x,T);
        mu = model_mu(x,T);
        sigma = model_sigma(x,T);
        sigma_Mo = (g*(mu^4)/Mo/rho)^(1/3);

        if abs(sigma - sigma_Mo)<=1e-3
            d1=((Bo*sigma/g/rho)^0.5); % m
            d2=(((Ga*mu/rho)^2)/g)^(1/3); % m
            err = abs(d1-d2)/d1*100;
            if abs(d1-d2)<=1e-6
                sigue=0;
                clc
                dm=(d1+d2)/2; % m
                d_orif=(dm^3)*rho*g/6/sigma*1e3; % mm
                fprintf('Concentration = %2g%% weigth\nDiameter of orifice
= %2g mm\nError = %2g%%\n',x,d_orif,err);
            else
                if x<100
                    x=x+0.01;
                else
                    disp('ERROR: no values found for diameter');
                    sigue=0;
                end
            end
        else
            if x<100
                x=x+0.01;
            else
                disp('ERROR: no values found for surface tension');
                sigue=0;
            end
        end
    end
end
```

A.3.1. Function for fluid properties interpolation

```
function [fitresult, gof] = FIT_prop_3D(x_s, T_s, prop_tabla)
%CREATEFIT(X_S,T_S,PROP_TABLA)
%  Create a fit.
%
%  Data for prop_3D' fit:
%      X Input : x_s
%      Y Input : T_s
%      Z Output: prop_tabla
%  Output:
%      fitresult : a fit object representing the fit.
%      gof : structure with goodness-of fit info.
%
%  See also FIT, CFIT, SFIT.

%  Auto-generated by MATLAB on 11-Mar-2019 17:38:40


%% Fit: 'prop_3D'.
[xData, yData, zData] = prepareSurfaceData( x_s, T_s, prop_tabla );

% Set up fittype and options.
ft = fittype( 'poly55' );
```

```
% Fit model to data.
[fitresult, gof] = fit( [xData, yData], zData, ft );

% % Plot fit with data.
% figure( 'Name', 'prop_3D' );
% h = plot( fitresult, [xData, yData], zData );
% legend( h, 'prop_3D', prop_tabla vs. x_s, T_s', 'Location', 'NorthEast'
);
% % Label axes
% xlabel x_s
% ylabel T_s
% zlabel prop_tabla
% grid on
% view( -125.5, 46.8 );
```

A.3.2. Function for real conditions of mixture calculation

```
clear
g = 9.81;
t = 24.3; %°C
T = t+273.15;
x = 0.7305;
v = ;
d = ((6*v/pi)^(1/3))/1000;
mu = 26.32/1000;

datos;
[model_rho, ~] = FIT_rho_3D(x_rho, T_rho, rho_tabla);
[model_sigma, ~] = FIT_sigma_3D(x_s, T_s, sigma_tabla);

rho = model_rho(x,T);
sigma = model_sigma(x,T);

Bo = rho*g*(d^2)/sigma;
Mo = g*(mu^4)/rho/(sigma^3);
Ga = ((Bo^3)/Mo)^.25;
```

A.4. Arduino code for camera control

```
//VARIABLES:

// inicialización de las entradas y salidas :

int entrada=4;

int led=13;

int salida=2;

int llenado=8;
```

```
// Inicialización de los parámetros característicos

int DelayTime=4000; //tiempo de espera en ms para que el sistema no admita entradas

int Open=30; //tiempo de apertura de la electroválvula

int Estable=6000; // tiempo necesario para que se estabilice el arduino en ms

int wait=500; //tiempo que hay que esperar para que el bórtice salga a tiempo en ms

void setup() {

pinMode(entrada,INPUT);

pinMode(led,OUTPUT);

pinMode(salida, OUTPUT);

pinMode(llenado,INPUT);

delay(Estable);

}

void loop() {

if (digitalRead(entrada)==1){

delay(wait);//tiempo de espera para la interacción
%%%%%%%%%%%%%%%%%%%%%%%%%%%%%%%%%%%%%%%%%%%

digitalWrite(led,HIGH);

digitalWrite(salida,HIGH);

delay(Open);// tiempo que está abierta la electroválvula

digitalWrite(salida,LOW);
```

```
delay(DelayTime);//tiempo que el sistema no admite señales de entrada; %%%%%%%%%%%%%%%%%%%%

digitalWrite(led,LOW);

}

if (digitalRead(llenado)==1) {

digitalWrite(salida,HIGH);

digitalWrite(led,HIGH);

}

else if (digitalRead(llenado)!=1){

digitalWrite(salida,LOW);

digitalWrite(led,LOW);

}



}
```